Phase diagram of a square Ising model with exchange and dipole interactions: Monte Carlo simulations

E. Rastelli,* S. Regina, and A. Tassi
Dipartimento di Fisica dell'Università di Parma, Parco Area delle Scienze 7/A, 43100 Parma, Italy
(Received 26 February 2007; revised manuscript received 5 June 2007; published 21 August 2007)

The thermal behavior of the square Ising model with exchange (J) and dipole (g) interactions is well understood for values of J/g far from the phase boundaries between striped configurations of different widths h. A variety of phase transitions were found by Monte Carlo simulations. Both first order and continuous phase transitions were found depending on the value of the ratio J/g, but no intermediate phase was found between the low temperature ordered striped phase and the high temperature paramagnetic one. Here, we investigate the regions of J/g near the boundaries between the striped phases of width h and $h+1$. We find that for $h=2,3$, an intermediate (modulated) phase occurs between the striped and paramagnetic phases. Of particular interest is the region around the boundary between the Néel phase and the striped phase with $h=1$ where an infinite sequence of $\langle 1,n\rangle$ ($\langle n,1\rangle$) configurations, never seen before, are found to become stable. They are characterized by horizontal (vertical) stripes made up of n identical antiferromagnetic rows (columns) alternated with n antiferromagnetic rows (columns) of spins reversed. The accumulation point of this sequence ($n\to\infty$) corresponds to the striped phase with $h=1$ (columnar phase).

DOI: 10.1103/PhysRevB.76.054438 PACS number(s): 75.10.Hk, 75.40.Cx, 75.40.Mg, 05.10.Ln

I. INTRODUCTION

The square Ising model with ferromagnetic nearest neighbor (NN) exchange interaction (J) and dipole (g) interaction has been extensively investigated[1–5] because of its theoretical interest in studying the effect of long range interactions in the critical region and in view of its possible application in describing the qualitative features of the spin configurations observed in ultrathin films of magnetic atoms on metal substrates.

Assuming that the spins are aligned perpendicularly to the plane, at increasing J/g, the zero temperature configuration changes from a Néel (N) configuration for $J=0$ to a ferromagnetic (F) configuration for $g=0$ passing through a sequence of $\langle h\rangle$ "striped phases" characterized by alternate stripes made up of h rows (columns) of spins up and down. The width of the stripes increases with J/g from $h=1$ (columnar phase) to $h\to\infty$ (F phase).

Here, we find that between the N configuration and the columnar phase $\langle 1\rangle$, an infinite sequence of configurations $\langle 1,n\rangle$ ($\langle n,1\rangle$) with $n=1,2,\ldots,\infty$ occurs. These configurations, never seen before, are characterized by horizontal (vertical) stripes made up of n identical antiferromagnetic rows (columns) followed by n antiferromagnetic rows (columns) of overturned spins.

At finite temperature, the model was extensively investigated by Monte Carlo (MC) simulation, and some general aspects have been well understood. For values of J/g far from the boundary between striped phases $\langle h\rangle$ and $\langle h+1\rangle$, a direct transition from the low temperature ordered phase to the high temperature paramagnetic phase was found.[3,4,6] On the contrary, in the neighborhood of the boundary between $\langle h\rangle$ and $\langle h+1\rangle$, an intermediate "modulated" phase may enter between the $\langle h\rangle$ and the paramagnetic phase. The modulated phase is characterized by an order wave vector $\boldsymbol{Q}$ intermediate between the commensurate wave vector characterizing the nearby striped phases $\langle h\rangle$ and $\langle h+1\rangle$. We show that the modulated phase occurs near the boundaries $\langle 2\rangle-\langle 3\rangle$ and $\langle 3\rangle-\langle 4\rangle$ but not at the boundary $\langle 1\rangle-\langle 2\rangle$.

In the literature, the striped, modulated, and paramagnetic phases are sometimes referred as smectic, nematic, and tetragonal. Indeed, the existence of "smectic crystal," "Ising nematic," and "tetragonal liquid" phases was conjectured studying a microscopic ferromagnetic exchange Hamiltonian with dipole interaction and easy-axis anisotropy describing ultrathin ferromagnetic films in the continuum limit.[7] Even though the model studied by Abanov *et al.*[7] differs significantly from the two-dimensional ferromagnetic Ising model with dipole interaction, the analogy between the smectic phase and the striped phase and the tetragonal phase and the disordered phase just above the transition temperature was discussed.[8] In particular no trace of the nematic phase was found for $J/g=6$ ($h=4$) and $J/g=8.9$ ($h=8$).[8] Support to the scenario where the striped phase goes directly into the tetragonal phase was given by several authors.[2,4,8] Later on, Cannas *et al.*[5] predicted the existence of a nematic phase between the striped and tetragonal one for stripes large enough on the basis of a MC simulation for $J/g=4$ ($h=2$). On the contrary, a direct transition from the striped to the tetragonal phase is expected[5] for thin stripes as confirmed by MC simulation for $J/g=2$ ($h=1$).

The layout of this paper is the following: In Sec. II, we obtain the zero temperature energy of the $\langle 1,n\rangle$ phases. In Sec. III, we present and discuss our MC simulations. In Sec. IV, we give the phase diagram of the model, and Sec. V is devoted to the conclusions.

II. ZERO TEMPERATURE ENERGY

The Hamiltonian of the model is

$$\mathcal{H}=-J\sum_{\langle i,j\rangle}\sigma_i\sigma_j+g\sum_{i\neq j}\frac{1}{r_{ij}^3}\sigma_i\sigma_j, \tag{1}$$

where the first sum is restricted to distinct pairs of NN spins and a ferromagnetic interaction $J>0$ is assumed; in the sec-

TABLE I. Coefficients a and b of the zero temperature energy $E_{\langle 1,n\rangle}/(gL^2)=a(J/g)+b$ for several $\langle 1,n\rangle$ phases.

n	a	b	Region of stability
1	2	−2.6458865323	(0, 0.83040611)
2	1	−1.8154804206	(0.83040611, 0.87883981)
3	2/3	−1.5225338186	(0.87883981, 0.88055814)
4	1/2	−1.3757741285	(0.88055814, 0.88062192)
5	2/5	−1.2877119365	(0.88062192, 0.88062437)
6	1/3	−1.2290036451	(0.88062437, 0.88062447)
7	2/7	−1.1870691466	(0.880624468, 0.880624472)
8	1/4	−1.1556182726	(0.8806244718, 0.8806244720)
9	2/9	−1.1311564817	(0.88062447197, 0.88062447198)
10	1/5	−1.1115870490	(0.8806244719811, 0.8806244719814)
$n\to\infty$	$2/n$	$-0.93546215-1.7612489/n$	$J/g>0.88062447198136$

ond sum, i and j run over all the sites of a square lattice $L\times L$. The spins $\sigma_i=\pm 1$ are supposed to be aligned out of plane. The analytic investigation of the zero temperature energy of Eq. (1) leads to a variety of configurations.

Assuming a double periodic spin configuration with period $2h_1$ along the x axis and $2h_2$ along the y axis, the zero temperature energy is

$$\frac{E_{\langle h_1,h_2\rangle}}{gL^2}=-2\frac{J}{g}\left(1-\frac{1}{h_1}-\frac{1}{h_2}\right)+\sum_{s_1=0}^{h_1-1}\sum_{s_2=0}^{h_2-1}\frac{D^{zz}\left[\frac{2\pi}{h_1}\left(s_1+\frac{1}{2}\right),\frac{2\pi}{h_2}\left(s_2+\frac{1}{2}\right)\right]}{h_1^2h_2^2\sin^2\left[\frac{\pi}{h_1}\left(s_1+\frac{1}{2}\right)\right]\sin^2\left[\frac{\pi}{h_2}\left(s_2+\frac{1}{2}\right)\right]}, \tag{2}$$

where

$$D^{zz}(\boldsymbol{Q})=\sum_{\boldsymbol{r}\neq 0}\frac{e^{i\boldsymbol{Q}\cdot\boldsymbol{r}}}{r^3}, \tag{3}$$

with $\boldsymbol{Q}=\left(\frac{2\pi}{L}Q_x,\frac{2\pi}{L}Q_y\right)$ with $Q_x,Q_y=0,1,2,\ldots,L-1$ and $\mathbf{r}=l\mathbf{u}_x+m\mathbf{u}_y$ (l, m are integers). The details of the calculation are given in Appendix A. We find that the $\langle h_1,h_2\rangle$ "checkerboard" configurations with both h_1 and $h_2\neq 1$ are never stable with respect to the $\langle 1,n\rangle$ or $\langle n,1\rangle$ phases with n arbitrary or with respect to the striped phases $\langle h\rangle$ obtained for $h_1\to\infty$ and $h_2=h$ or $h_1=h$ and $h_2\to\infty$. The zero temperature energy of the striped $\langle h\rangle$ phase is

$$\frac{E_{\langle h\rangle}}{gL^2}=-2\frac{J}{g}\left(1-\frac{1}{h}\right)+\frac{1}{h^2}\sum_{s=0}^{h-1}\frac{D^{zz}\left[\frac{2\pi}{h}\left(s+\frac{1}{2}\right),0\right]}{\sin^2\left[\frac{\pi}{h}\left(s+\frac{1}{2}\right)\right]}. \tag{4}$$

In Table I, we give the region of stability for several $\langle 1,n\rangle$ phases. The zero temperature Néel configuration $\langle 1,1\rangle$ is stable for $J/g<0.830\,406$. For $0.830\,406<J/g<0.880\,62$, an infinite sequence of phases $\langle 1,n\rangle$, with $n=2,3,\ldots$, appears. These phases are characterized by stripes of n identical antiferromagnetic rows followed by as many antiferromagnetic rows of overturned spins. For $n=1$, the checkerboard phase reduces to the N configuration $\langle 1,1\rangle$; for $n=\infty$, the checkerboard phase reduces to the striped configuration $\langle 1\rangle$ corresponding to a "columnar phase" in which ferromagnetic columns of spins up and down alternate. The width of the stripes made up with antiferromagnetic rows becomes larger as J/g increases from 0.83 to 0.88. For $n\to\infty$, the zero temperature energy becomes

$$\frac{E_{\langle 1,n\rangle}(n\to\infty)}{gL^2}=\frac{2}{n}\frac{J}{g}-0.935\,462\,154\,6-\frac{1.761\,248\,944}{n}+O\left(\frac{1}{n^2}\right), \tag{5}$$

as shown in Appendix A. Note that for $J/g=0.880\,862\,447\,2$, the energy of the $\langle 1,n\rangle$ phase is independent of n neglecting terms of order $1/n^2$. This accumulation point is similar to the multiphase point ($T=0$, $J_2/J_1=-1/2$) found in the anisotropic next nearest neighbor Ising (ANNNI) model[9] in two and three dimensions, where the competition between the nearest neighbor (NN) interaction J_1 and the next nearest neighbor interaction J_2 is restricted to one direction (i.e., the x axis) of a square or a simple cubic lattice.

In Fig. 1, we show the configurations $\langle 1,2\rangle$, $\langle 1,3\rangle$, and $\langle 1,4\rangle$ for a square lattice of side $L=48$. The white and black squares correspond to spins of opposite orientations. The corresponding structure factor

$$S(\boldsymbol{Q})=\frac{|\sigma_{\boldsymbol{Q}}|^2}{L^2},\quad \sigma_{\boldsymbol{Q}}=\frac{1}{L}\sum_i\sigma_i e^{i\boldsymbol{Q}\cdot\boldsymbol{r}_i} \tag{6}$$

is shown on the right of each configuration. As one can see, the $\langle 1,n\rangle$ phase is an "irregular" checkerboard, where the squares are replaced by rectangles that are large one lattice unit and high n lattice units. A checkerboard configuration was proposed as possible zero temperature configuration for the present model by Czech and Villain[10] in the limit of large

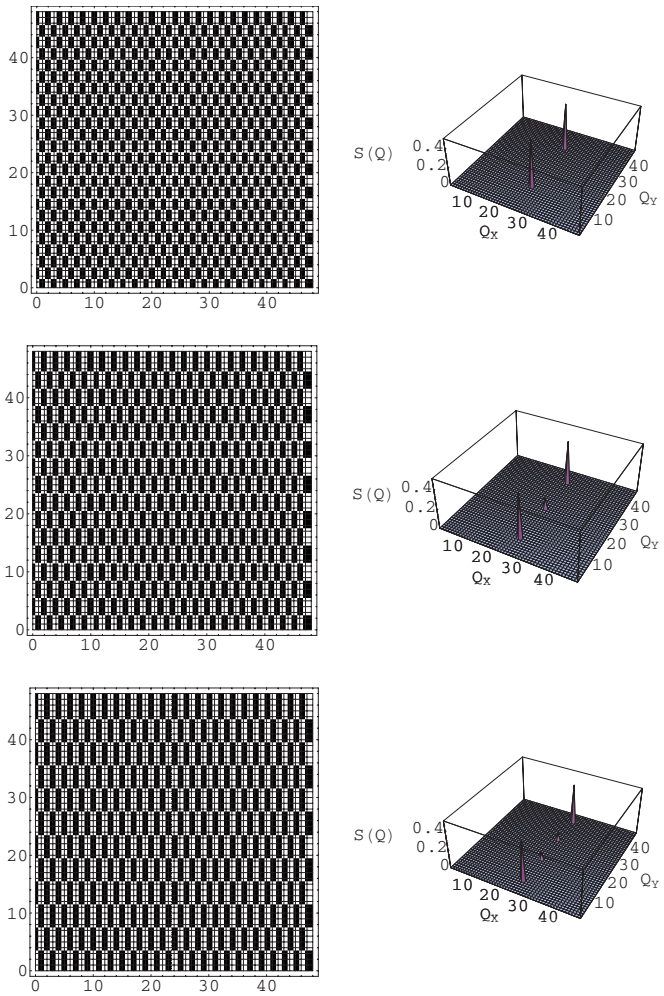

FIG. 1. (Color online) Zero temperature configuration of the phases $\langle 1,2\rangle$ (upper panel), $\langle 1,3\rangle$ (middle panel), and $\langle 1,4\rangle$ (lower panel) with the corresponding structure factors $S(Q)$.

J/g. They arrived at the conclusion that for $\langle m,n\rangle$ configurations with $m,n\to\infty$, the zero temperature energy was characterized by $m=n$ that is a "regular" checkerboard configuration. On the other hand, striped configurations are believed to be lower in energy with respect to the checkerboard ones.[6] Anyway, for J/g not too large (small n, m), the previous analysis does not apply and a direct comparison of the energies of the different spin configurations is in order. Indeed, we find that irregular checkerboard phases $\langle 1,n\rangle$ have an energy lower than the striped phases in a narrow region of J/g located between the N and $\langle 1\rangle$ phase. Any other checkerboard configuration $\langle m,n\rangle$ with $m\neq 1$ is never stable for any J/g.

For J/g increasing from 0.880 62, a sequence of striped configurations $\langle h\rangle$, with $h=1,2,\ldots$, occurs until the ferromagnetic phase F corresponding to $h\to\infty$ is reached. In Table II, we give the region of stability of the $\langle h\rangle$ striped phases.

As shown in Appendix A for large h, the energy of the striped configuration $\langle h\rangle$ is given by

$$\frac{E_{\langle h\rangle}(h\to\infty)}{gL^2} = -2\frac{J}{g}\left(1-\frac{1}{h}\right) + 9.033\,622 - \frac{8}{h}\ln h - \frac{9.143\,326}{h} + O\left(\frac{1}{h^2}\right), \tag{7}$$

so that the transition between the F phase and the largest striped phase $\langle L/2\rangle$ occurs at $J/g=1.799\,074+\ln L^4$.

III. MONTE CARLO SIMULATION

We perform MC simulations on a square lattice of side $L=48$ with periodic boundary conditions. The choice of a size 48×48 is suggested by the fact that such a lattice supports stripes of width $h=1,2,3,4,6,8,12,24$.

In Table III, we give the zero temperature energies and the stability regions of the $\langle 1,n\rangle$ and $\langle h\rangle$ configurations consistent with the lattice of side $L=48$. Comparing Table III with Tables I and II, one can see the limitations entered by a finite lattice with periodic boundary conditions. The main effect of the finite lattice size is to dramatically reduce the number of checkerboard or striped phases permitted. Indeed, for phases with $n\leqslant 4$ or $h\leqslant 4$, no difference is noted between the zero temperature energy sequence and the stability regions of the "infinite" lattice and of the lattice with $L=48$. For higher n or h, the "finite" lattice prevents the occurrence of phases with $L/(2n)$ or $L/(2h)$ not equal to an integer number so that, for instance, striped phases such as $\langle 4\rangle$ and $\langle 6\rangle$ or $\langle 6\rangle$ and $\langle 8\rangle$ become adjoining. We have found that stripelike nonperiodic configurations reminiscent of the striped phases prevented by the finite size of the lattice may appear. Indeed, if we write the more general zero temperature energy of a stripelike configuration for a square lattice of side L,

$$E = \sum_{Q_x=0}^{L-1}\left[-J\left(1+\cos\frac{2\pi}{L}Q_x\right) + gD^{zz}\left(\frac{2\pi}{L}Q_x,0\right)\right]S\left(\frac{2\pi}{L}Q_x,0\right), \tag{8}$$

where $S\left(\frac{2\pi}{L}Q_x,0\right)$ is the finite Fourier transform defined in Eq. (6), we are able to give the energy for an arbitrary stripelike configuration. For $L=48$, we recover all the energies shown in Table III assuming a regular striped configuration. In addition, we have found that a configuration consisting of two stripes of width $h=4$ followed by eight stripes of width $h=5$ ($\langle 4^2 5^8\rangle$) becomes stable in the range $6.63<J/g<7.23$. Let us call this phase $\langle\sim 5\rangle$. An analogous $\langle\sim 7\rangle$ phase might be expected between the striped phases $\langle 6\rangle$ and $\langle 8\rangle$, but any attempt to find such a phase was unsuccessful. Indeed, phases such as $\langle 5^4 7^4\rangle$, $\langle 5^3 6^3 7^2\rangle$, and $\langle 10^2 7^4\rangle$ have a zero temperature energy higher than, even though very close, to the regular striped phases $\langle 6\rangle$ or $\langle 8\rangle$. The lattice size $L=48$ is too small to allow a stripelike configuration of that type. We performed the same investigation on a lattice with $L=32$ for which the only possible (regular) striped phases are characterized by $h=1,2,4,8,16$. We found that a phase $\langle 3^9 5\rangle=\langle\sim 3\rangle$ occurs between the striped phases $\langle 2\rangle$ and $\langle 4\rangle$ for $4.56<J/g<5.41$. Analogously, a phase $\langle 5^4 6^2\rangle$ appears

TABLE II. Coefficients a and b of the zero temperature energy $E_{\langle h\rangle}/(gL^2)=a(J/g)+b$ for striped configurations of width h.

h	a	b	Region of stability
1	0	−0.9354621546	(0.880625,2.517077)
2	−1	1.5816148819	(2.517077,4.344909)
3	−4/3	3.0299178788	(4.344909,5.628990)
4	−3/2	3.9680829288	(5.628990,6.608484)
5	−8/5	4.6893131395	(6.608484,7.398049)
6	−5/3	5.1221346075	(7.398049,8.058698)
7	−12/7	5.5058821312	(8.058698,8.626345)
8	−7/4	5.8139658640	(8.626345,9.123814)
9	−16/9	6.0674051477	(9.123814,9.566483)
10	−9/5	6.2799936626	(9.566483,9.965190)
11	−20/11	6.4611789296	(9.965190,10.327855)
12	−11/6	6.6176615768	(10.327855,10.660440)
13	−24/13	6.7543338863	(10.660440,10.967544)
14	−13/7	6.8748563518	(10.967544,11.252788)
15	−28/15	6.9820257605	(11.252788,11.519072)
16	−15/8	7.0780180265	(11.519072,11.768757)
17	−32/17	7.1645530020	(11.768757,12.003788)
18	−17/9	7.2430091326	(12.003788,12.225789)
19	−36/19	7.3145049739	(12.225789,12.436127)
20	−19/10	7.3799582736	(12.436127,12.635966)
21	−40/21	7.4401295385	(12.635966,12.826302)
22	−21/11	7.4956546573	(12.826302,13.007999)
23	−44/23	7.5470696747	(13.007999,13.181806)
24	−23/12	7.5948298428	(13.181806,13.348380)
$h\to\infty$	$-2(1-1/h)$	$9.033622-(8/h)\ln h-9.143326/h$	$J/g>1.799074+\ln L^4$

for $6.77<J/g<7.99$ between the striped phases $\langle 4\rangle$ and $\langle 8\rangle$.

For this reason, we restrict our investigation to the checkerboard phases with $n\leqslant 3$ or striped phases with $h\leqslant 4$. Note that for phases $\langle 1,n\rangle$ with $n>8$, the region of stability is so small that it cannot be shown within the numerical precision of the table. For a lattice of side $L=48$, the striped configuration with the widest stripe corresponds to $\langle 24\rangle$, so that the phase boundary between the largest striped and the F phase becomes $J/g=17.27$. We have also performed extensive MC simulations in the F region for $20<J/g<100$.

A. Method and observables

We perform at least eight independent MC runs starting from the low temperature configuration. In each run, we increase the temperature of 0.01 (in units of g/k_B) taking the last configuration of the previous temperature as the initial configuration of the next one and disregarding 10^4 Monte Carlo steps (MCSs) for equilibration. For each temperature, we select 10^4 configurations over 10^5 MCSs and we evaluate the specific heat

$$C=\frac{\langle\mathcal{H}^2\rangle-\langle\mathcal{H}\rangle^2}{L^2k_BT^2}, \tag{9}$$

the internal energy per spin in units of dipolar interaction

$$E=\frac{\langle\mathcal{H}\rangle}{L^2g}, \tag{10}$$

and the order parameter[8]

$$O_{hv}=\left\langle\left|\frac{n_h-n_v}{n_h+n_v}\right|\right\rangle, \tag{11}$$

where n_h (n_v) is the number of horizontal (vertical) pairs of NN antiparallel spins. Note that this parameter is zero in the N phase where it is replaced by the conventional staggered magnetization.[4] Then, we evaluate the average $\langle S(\boldsymbol{Q})\rangle$, where $S(\boldsymbol{Q})$ is the structure the factor given by Eq. (6). We have checked that any step observed in the order parameter O_{hv} vs temperature corresponds to a shift of the main peak of the structure factor $\langle S(\boldsymbol{Q})\rangle$ that is to a change of the order wave vector characterizing the spin configuration. The order parameter O_{hv}, originally introduced[8] to describe the long range order of a stripe configuration, may be convenient to point out a possible transition to a modulated phase and finally to a disordered phase. To determine the nature of the transition, a crucial role is played by the energy density distribution $P(E)$: The occurrence of a two-peak structure in $P(E)$ at some temperature is a strong indication of a first

TABLE III. Coefficients a and b of the zero temperature energies for $\langle 1,n\rangle$ and $\langle h\rangle$ configurations compatible with a square lattice of side $L=48$.

h	a	b	Region of stability
$\langle 1,1\rangle$=N	2	−2.6458865323	(0, 0.830406)
$\langle 1,2\rangle$	1	−1.8154804206	(0.830406, 0.878840)
$\langle 1,3\rangle$	2/3	−1.5225338186	(0.878840, 0.880558)
$\langle 1,4\rangle$	1/2	−1.3757741285	(0.880558, 0.880622)
$\langle 1,6\rangle$	1/3	−1.2290036451	(0.880622, 0.880624)
$\langle 1,8\rangle$	1/4	−1.1556182726	J/g=0.880624
$\langle 1,\infty\rangle=\langle 1\rangle$	0	−0.9354621546	(0.880624, 2.517077)
$\langle 2\rangle$	−1	1.5816148819	(2.517077, 4.344909)
$\langle 3\rangle$	−4/3	3.0299178788	(4.344909, 5.628990)
$\langle 4\rangle$	−3/2	3.9680829288	(5.628990, 6.924310)
$\langle 6\rangle$	−5/3	5.1221346075	(6.924310, 8.301975)
$\langle 8\rangle$	−7/4	5.8139658640	(8.301975, 9.644349)
$\langle 12\rangle$	−11/6	6.6176615768	(9.644349, 11.726019)
$\langle 24\rangle$	−23/12	7.5948298428	(11.726019, 17.265502)
$\langle\infty\rangle$=F	−2	9.0336216831	$J/g>17.265502$

order transition at that temperature.[11] As for the order parameter density distribution[3] $P(O_{hv})$, it is more convenient to neglect the absolute value in Eq. (11) since the tetragonal phase,[1] characterized by a free rotation of the stripes from horizontal to vertical or vice versa, implies a change of sign of the order parameter O_{hv} so that if the absolute value is omitted, a two-peak structure in $P(O_{hv})$ is expected when the tetragonal phase occurs.

The phase transitions between the striped phase and the modulated phase and between the modulated and tetragonal phases are both first order[5] for $J/g=4$ ($h=2$). Cannas *et al.*[5] arrived at this conclusion after having performed very long single run MC simulations: Runs of $2\times10^7-2\times10^8$ MCSs disregarding 10^6-10^7 configurations for equilibration starting from a random configuration were performed on a square lattice of side $L=56$. Note that each MCS (L^2 spin-flip trials) takes about 0.02–0.03 s for lattices of size $48\times48-56\times56$, since the long range nature of the dipole interaction between the spins implies that the computer time is proportional to L^4 instead of L^2 for a system with short range interactions.

On the contrary, we have performed independent series of much shorter MC runs (eight or more independent MC runs of 10^5 MCSs) increasing temperature from zero. Starting from low temperature, we take advantage of the knowledge of the exact zero temperature configuration of the system so that the equilibrium configuration is reached soon. Moreover, increasing temperature by 0.01 at each step, we keep the system near the equilibrium configuration and the effective number of MCSs at the transition temperature is large enough to expect that the final configuration is similar to that obtained using a much longer MC time series starting from a random configuration.

The "short" runs used in our MC simulations allow us to investigate a wide spectrum of values of J/g so that a realistic phase diagram of the model can be drawn. The reliability of our method was checked comparing our results with those of Cannas *et al.*[5] for $J/g=4$. We find an overall agreement with the data[5] obtained performing much longer single run MC simulations. Indeed, our independent runs are nearly the same for values of J/g not too close to the phase boundaries so that the average over the independent runs leads to very small error bars in the specific heat and order parameter. On the contrary, in the proximity of the boundaries between striped phases of different widths, the error bars become larger for two reasons: The transition temperature at which the specific heat shows a very narrow peak, typical of a first order phase transition, changes slightly from one run to another; for instance, the error affecting the transition temperature is less than 0.01 around the boundary $\langle 1\rangle-\langle 2\rangle$, and it becomes 0.05 at the $\langle 2\rangle-\langle 3\rangle$ boundary and 0.1 at the $\langle 3\rangle-\langle 4\rangle$ boundary. The uncertainty on the transition temperature, even though small, implies that the average over independent runs broadens the peak of the specific heat reducing its height. The second source of error concerns the height of the peak which differs from one run to another. Indeed, we have checked that the peak height is crucially dependent on the amount of the coexisting phases at the transition temperature leading to a wide spectrum of values of the specific heat maximum. Analogous considerations can be done for the steps in the order parameter. To reduce the uncertainty on the transition temperature and the error bar on the height of the specific heat peak, one could reduce the temperature step between one simulation and the next one and (or) take longer simulations. However, since we are interested in the phase diagram and in the nature of the transition, the precise location of the transition temperature and the careful determination of the height of the specific heat maximum are beyond the aim of the present work.

A nugget of information we receive from the "single run" inspection is that *each run* shows a very narrow peak in the specific heat even though its location and height fluctuate from one run to another. For this reason, we investigate the phase transition by looking at the density distribution of the energy $P(E)$ and of the order parameter $P(O_{hv})$ together with the structure factor $\langle S(\boldsymbol{Q})\rangle$ obtained from the time series of a single run MC simulation. Notice that a two-peak structure of the energy density distribution, as well as a three-peak structure of the order parameter density distribution, gives a strong indication of a first order phase transition.[3,5,11]

As for the specific heat and the order parameter vs temperature, we have performed an average over at least eight independent runs to get reliable equilibrium results. Then, we choose the time series of the run for which the location and height of the specific heat peak are closer to the average in order to study the behavior of the density distributions $P(E)$, $P(O_{hv})$, and the structure factor $\langle S(\boldsymbol{Q})\rangle$.

B. Néel and $\langle 1,n\rangle$ phases

For the Néel antiferromagnetic (N) phase ($0<J/g<0.8304$), we see that the specific heat vs temperature shows a peak typical of a continuous phase transition located at temperatures that decrease when J/g increases. For in-

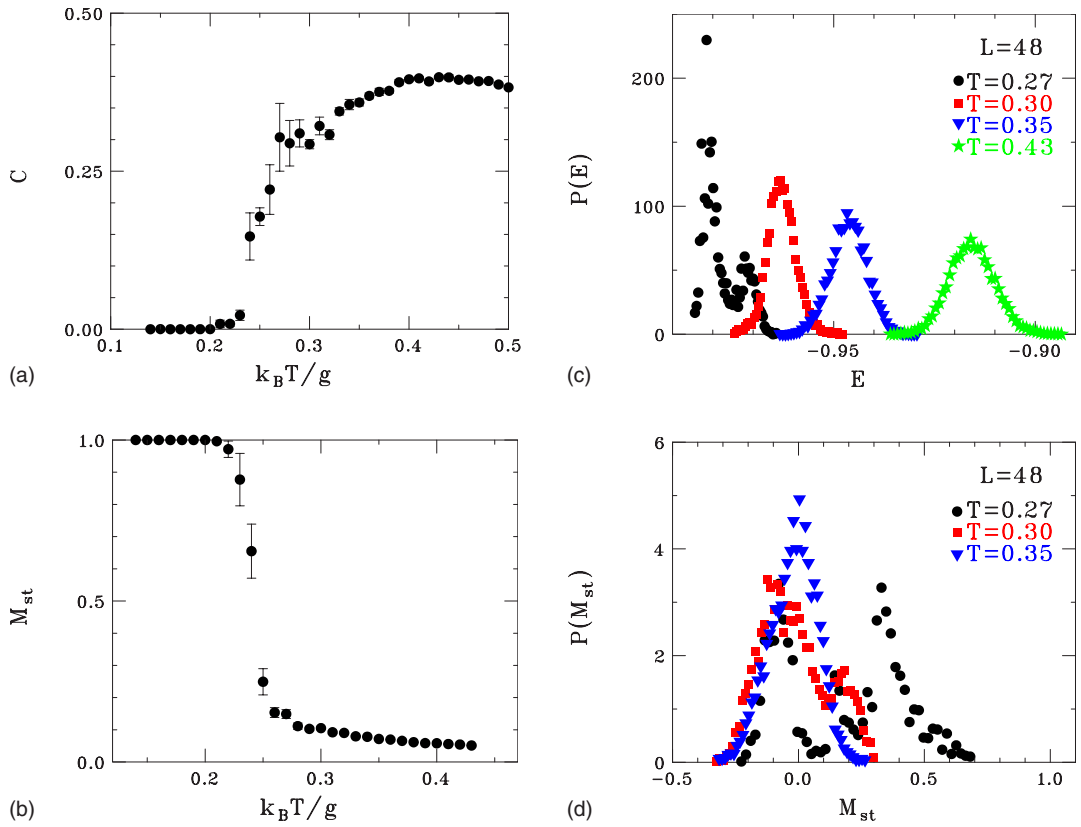

FIG. 2. (Color online) (a) Specific heat and (b) sublattice magnetization vs temperature for $J/g=0.83$ (Néel phase); (c) energy density distribution $P(E)$ and (d) order parameter density distribution $P(M_{st})$ for selected temperatures.

stance, we find $k_BT/g=2.38,1.19,0.67,0.36$ for $J/g=0,0.5,0.7,0.8$. The shape of the specific heat changes approaching the transition between the N and $\langle 1,2\rangle$ phase. This unconventional behavior is shown in Figs. 2(a) and 2(b) where the specific heat and the order parameter M_{st} (staggered magnetization) vs temperature are given for $J/g=0.83$. An abrupt increase of the specific heat, as well as a sudden drop of the sublattice magnetization at $k_BT/g\simeq 0.25$, is clearly seen. In Figs. 2(c) and 2(d), we show the energy and order parameter density distribution for a single run that shows a peak height of 0.67 in the specific heat at $k_BT/g=0.27$. A two-peak structure in both the energy and sublattice magnetization density distribution is seen at $k_BT/g=0.27$. Notice that for $k_BT/g\lesssim 0.23$, the δ-like peak of $P(E)$ is located at $E=-0.986$, undistinguishable from the value $E=-0.985\,89$ deduced from the analytic result of Table I at $T=0$. For $k_BT/g\lesssim 0.23$, the δ-like peak of $P(M_{st})$ is located at $M_{st}\simeq 1$. In the same range of temperature, the structure factor shows a δ-like peak of intensity $\simeq 1$ located at the antiferromagnetic wave vector $\boldsymbol{Q}=(\pi,\pi)$. At $k_BT/g=0.24$, the height of the peak reduces to 0.65 even though its location does not change. For $0.25<k_BT/g<0.27$, a ridgelike structure appears whose maximum, located at $\boldsymbol{Q}=(\pi,\pi)$, is $\simeq 0.09$. Such a structure is similar to that shown in the middle panel of Fig. 3. For $k_BT/g>0.27$, a crosslike structure of $\langle S(\boldsymbol{Q})\rangle$ centered about $\boldsymbol{Q}=(\pi,\pi)$ appears with intensity further reduced to less than 0.01. In Fig. 3, we show three snapshots that illustrate the more significant configurations observed at $k_BT/g=0.27$. On the right of each snapshot, the corresponding structure factor $S(\boldsymbol{Q})$ is reported. The upper and lower panels represent configurations corresponding to the peak on the left of the energy and order parameter density distributions (black full circles) of Figs. 2(c) and 2(d). As one can see, any combination of the N phase ($\langle 1,1\rangle$) and $\langle 1,2\rangle$ occurs. The middle panel of Fig. 3 represents a configuration typical of the peak on the right of both $P(E)$ and $P(M_{st})$. The low intensity and the ridgelike shape of the structure factor (that becomes a crosslike shape similar to that shown in the middle panel of Fig. 5 for $k_BT/g\gtrsim 0.30$) point out the kind of *short range* order present in the disordered phase.

In Fig. 4, we show the same quantities as in Fig. 2 for $J/g=0.86$ ($\langle 1,2\rangle$ phase) except that the staggered magnetization M_{st} is replaced by the order parameter O_{hv} given by Eq. (11). In Figs. 4(a) and 4(b), we show the average over eight runs of the specific heat and the order parameter O_{hv} vs temperature. As one can see, the value of the order parameter at $T=0$ for the $\langle 1,2\rangle$ phase is 1/3. It is easy to see that the order parameter at $T=0$ for the phases $\langle 1,n\rangle$ is $O_{hv}=(n-1)/(n+1)$ going to 1 only at the accumulation point where the $\langle 1,n\rangle$ phases meet the striped phase $\langle 1\rangle$. The energy and order parameter density distribution shown in Figs. 4(c) and 4(d) are obtained from the time series of the single run with a specific heat peak height of 5.07 located at $k_BT/g=0.34$. For $k_BT/g=0.33$, the δ-like peaks in $P(E)$ at $E=-0.949$ and in $P(O_{hv})$ at $O_{hv}=0.327$ correspond to the ordered $\langle 1,2\rangle$ phase ($E=-0.955\,48$ and $O_{hv}=1/3$ at $T=0$). The structure factor shows two δ-like peaks of height of $\simeq 0.5$ located at

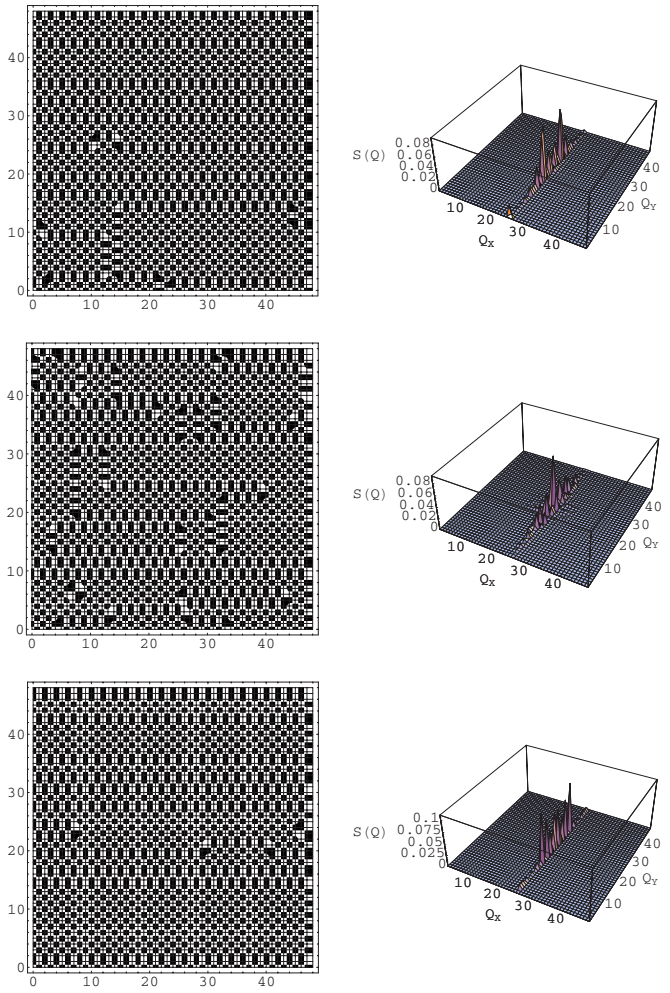

FIG. 3. (Color online) Snapshots and corresponding structure factors for $J/g=0.83$ and $k_BT/g=0.27$: $M_{st}=-0.107$, $E=-0.980$ (upper panel); $M_{st}=0.303$, $E=-0.969$ (middle panel); $M_{st}=-0.120$, $E=-0.983$ (lower panel).

$\boldsymbol{Q}=(\pi,\pm\pi/2)$ for $0<k_BT/g<0.30$. For $0.30<k_BT/g<0.33$, the peaks broaden and consequently reduce their intensity to 0.2–0.3. Finally, at $k_BT/g=0.34$, the $\langle 1,2\rangle$ and $\langle 2,1\rangle$ phases may be seen simultaneously, and the intensity of the peaks is reduced to less than 0.1. At $k_BT/g=0.34$, the energy and order parameter density distribution assume a broaden shape [(red) squares of Figs. 4(c) and 4(d)] even though a two-peak structure in $P(E)$ or a three-peak structure in $P(O_{hv})$, typical of a first order phase transition, is hardly singled out. Typical configurations corresponding to $k_BT/g=0.34$ are shown in Fig. 5.

A support of the existence of a first order transition between the $\langle 1,2\rangle$ phase and the tetragonal one can be caught by looking at the discontinuous shift in the location of the peaks of $P(E)$ and $P(O_{hv})$ moving from $k_BT/g=0.33$ to $k_BT/g=0.35$. The peaks at $k_BT/g=0.35$ correspond to the disordered phase as confirmed by the weak intensity (less than 0.01) and by the crosslike shape of the structure factor (see, for instance, the middle panel of Fig. 5).

In Fig. 6, we show the same quantities as in Fig. 4 for $J/g=0.88$. At $T=0$, the stable phase is the $\langle 1,3\rangle$ configuration shown in the lower panel of Fig. 1 with energy $E=-0.935\,87$ and order parameter $O_{hv}=1/2$. In Figs. 6(a) and 6(b), we show the average over eight runs of the specific heat and order parameter vs temperature. In Figs. 6(c) and 6(d), we show the density distributions $P(E)$ and $P(O_{hv})$ for the run whose specific heat peak is 3.60 high and located at $k_BT/g=0.36$. These distributions look very similar to those of Fig. 4 even though the three-peak structure of $P(O_{hv})$ for $k_BT/g=0.36$ is better singled out [see (red) squares in Fig. 6(d)]. In Fig. 7, we give three snapshots with the corresponding structure factors for $J/g=0.88$ and $k_BT/g=0.36$. In this case the configurations of the upper and lower panels are not easily amenable to the $\langle 1,3\rangle$ and $\langle 3,1\rangle$ phases. This is explained by the presence of the accumulation point $J/g=0.8806$ very close to the value at which we performed the MC simulation. Indeed, for $J/g\simeq 0.88$, any $\langle 1,n\rangle$ phase with $n>2$ has virtually the same energy as shown in Table I. Most of the phases have an order parameter $0.5<O_{hv}<0.7$, so that the bump in the order parameter observed in Fig. 6(b) before the sudden decrease at the transition can be explained. The structure factor shows three δ peaks at $\boldsymbol{Q}=(\pm\pi/3,\pi)$ (main peaks of intensity of 0.44) and $\boldsymbol{Q}=(\pi,\pi)$ with intensity 0.11 for $0<k_BT/g<0.20$. For $0.26<k_BT/g<0.36$, the peaks become a ridge of intensity less than 0.1, and for $k_BT/g>0.36$, the ridge becomes a cross of intensity $\simeq 0.01$.

C. Striped phases

We have performed many MC simulations for several J/g to draw a realistic phase diagram. The specific heat in the region of stability of the striped phase $\langle 1\rangle$ $(0.8804<J/g<2.5171)$ shows a maximum at $k_BT/g=0.51,0.58,0.80,0.83,0.80,0.53$, for $J/g=0.95,1,1.4,1.7,2,2.5$, respectively. The peak is very sharp (high about 10) near the boundary with the $\langle 1,n\rangle$ phase and with the $\langle 2\rangle$ striped phase. The peak is less pronounced (high about 2) and wider in the inner region. On the other hand, the error is less than 1% in the inner region and about 10% near the boundaries. As for the region of stability for the striped phase $\langle 2\rangle$ $(2.5171<J/g<4.3449)$, we find that the peak of the specific heat occurs at $k_BT/g=0.66,1.15,1.45,1.57,1.58,1.48$, for $J/g=2.6,3,3.4,3.7,4,4.3$, respectively. The peak is very sharp (high about 15) for $2.6<J/g<4$ and less pronounced for $J/g=4$ (3.7) and $J/g=4.3$ (0.5). At the transition, the error bars are between 2% and 30% (smaller errors are found for values of J/g far from boundaries). Moreover, for $J/g=4$ and 4.3, another peak at temperatures $k_BT/g=1.63$ and 1.68 (with an error within 1%) is recorded. In the region of stability of the striped phase $\langle 3\rangle$ $(4.3449<J/g<5.6290)$, the first peak of the specific heat occurs at $k_BT/g=1.51,1.93,2.12,2.16,2.14$ for $J/g=4.4,4.7,5,5.3,5.6$, respectively. A second peak at $k_BT/g=1.75,2.31,2.42$ is seen only for $J/g=4.4,5.3,5.6$ that is in the neighborhood of the boundaries between the striped phases $\langle 2\rangle-\langle 3\rangle$ and $\langle 3\rangle-\langle 4\rangle$. For this reason, we focus on values of J/g very near to the boundary of the stability region between the striped phases $\langle h\rangle$ and $\langle h+1\rangle$.

In Figs. 8 and 9, we give the specific heat, the order parameter, and the density distributions for $J/g=2.5$ $(h=1)$

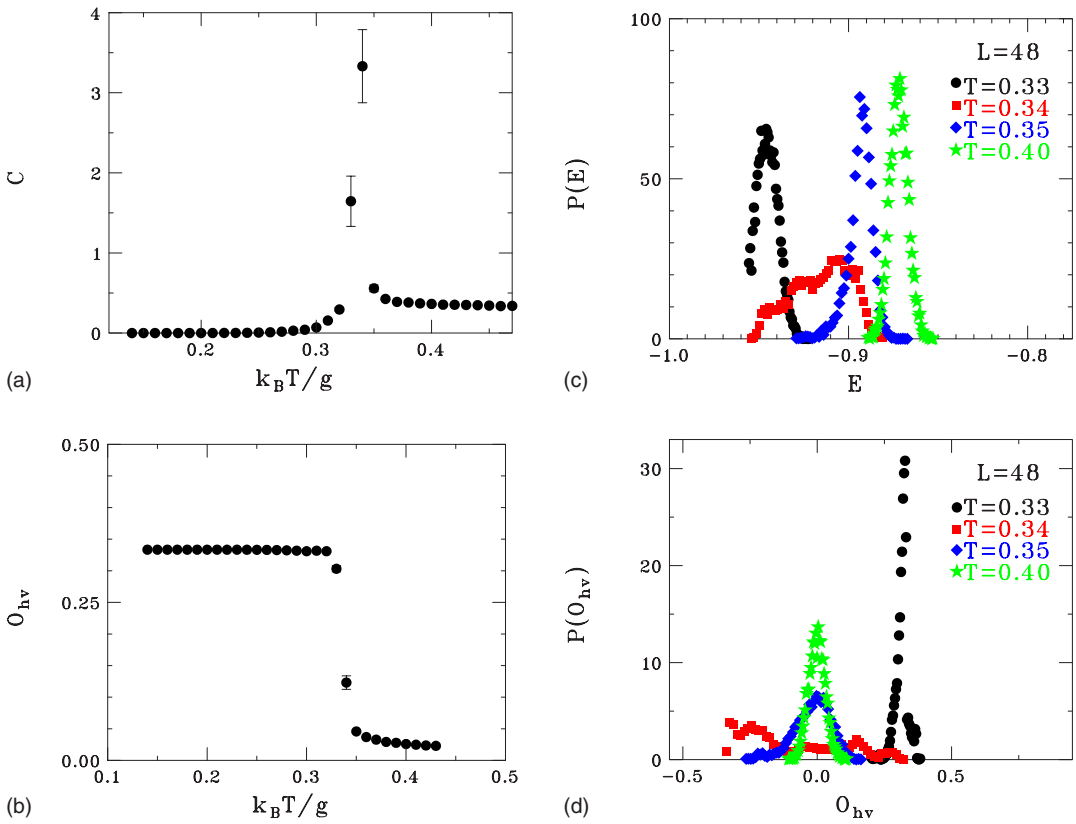

FIG. 4. (Color online) (a) Specific heat and (b) order parameter vs temperature for $J/g=0.86$ ($\langle 1,2\rangle$ phase); (c) energy density distribution $P(E)$ and (d) order parameter density distribution $P(O_{hv})$ for selected temperatures.

and 2.6 ($h=2$), respectively. For $J/g=2.5$, only one narrow peak in the specific heat at $k_BT/g=0.53$ is found as shown in Fig. 8(a). Also, the order parameter [Fig. 8(b)] shows a single step from the low temperature striped configuration ($O_{hv}\simeq 1$) to the high temperature paramagnetic phase ($O_{hv}\simeq 0$) at $k_BT/g=0.53$. This sudden drop of the order parameter suggests the occurrence of a first order transition. This conjecture is supported by the inspection of the single run time series. Selecting the single run with a peak in the specific heat of height of 17 located at $k_BT/g=0.53$, a discontinuous change in the location of the peak in the energy density distribution [Fig. 8(c)] is seen going from $k_BT/g=0.52$ [(black) full circles] to $k_BT/g=0.54$ [(blue) diamonds]. At $k_BT/g=0.53$ [(red) squares], a two-peak structure is hard to be identified even though a broad energy distribution between $E\simeq -0.93$ and $E\simeq -0.78$ is clearly seen. Notice the smooth displacement of the peak toward higher energy from $k_BT/g=0.54$ onward together with a narrowing of the peak itself. A similar behavior is observed in the order parameter density distribution $P(O_{hv})$ [Fig. 8(d)]: a discontinuous shift of the peak from $O_{hv}=-1$ to $O_{hv}=0$ is recorded passing from $k_BT/g=0.52$ to $k_BT/g=0.60$. We took many snapshots of the spin configurations during the time series at $k_BT/g=0.53$, as well as for lower and higher temperatures. In Figs. 8(e) and 8(f), we show two snapshots taken at $k_BT/g=0.53$: the former shows a striped configuration with $E=-0.930$, $O_{hv}=-0.993$ and it is the prototype of the low temperature phase, and the latter shows a configuration with $E=-0.780$, $O_{hv}=0.022$ typical of the high temperature tetragonal phase. The structure factors on the right show a δ-like peak for $\boldsymbol{Q}=(0,\pi)$ corresponding to the striped phase $\langle 1\rangle$ and a crown-shaped profile corresponding to the disordered phase. These two snapshots point out the coexistence of the striped phase $\langle 1\rangle$ with the tetragonal one at $k_BT/g=0.53$.

The scenario found for $J/g=2.5$ is enforced by the MC simulation performed at $J/g=2.6$, where the low temperature ordered configuration is the striped phase $\langle 2\rangle$. As one can see in Fig. 9, the onset of a first order phase transition between the striped and tetragonal phases is confirmed. Indeed, the two-peak structure in both $P(E)$ and $P(O_{hv})$ is well established at $k_BT/g=0.66$. The single run selected to give $P(E)$ and $P(O_{hv})$ shown in Fig. 9 has a specific heat peak height of 37.6 at $k_BT/g=0.66$. However, we have also evaluated $P(E)$ and $P(O_{hv})$ for other two single run time series: one having a peak height of 2.30 located at $k_BT/g=0.67$ and the other with the peak height of 15.5 located at $k_BT/g=0.66$. The scenario is the same as those illustrated in Figs. 9(c) and 9(d): A discontinuous shift in the location of the peak is seen at the transition. The main difference is that for the run with the highest specific heat peak, the two-peak structure of $P(E)$ is more pronounced since the two peaks have comparable intensity. Note that the specific heat peak is twice higher than that occurring at $J/g=2.5$, pointing out a stronger first order character of the transition. The snapshots taken at $k_BT/g=0.66$ show the coexistence of the striped configuration $\langle 2\rangle$ and the tetragonal phase which looks like very similar to that found from the simulation with $J/g=2.5$ as one can see from comparing Figs. 8(f) and 9(f).

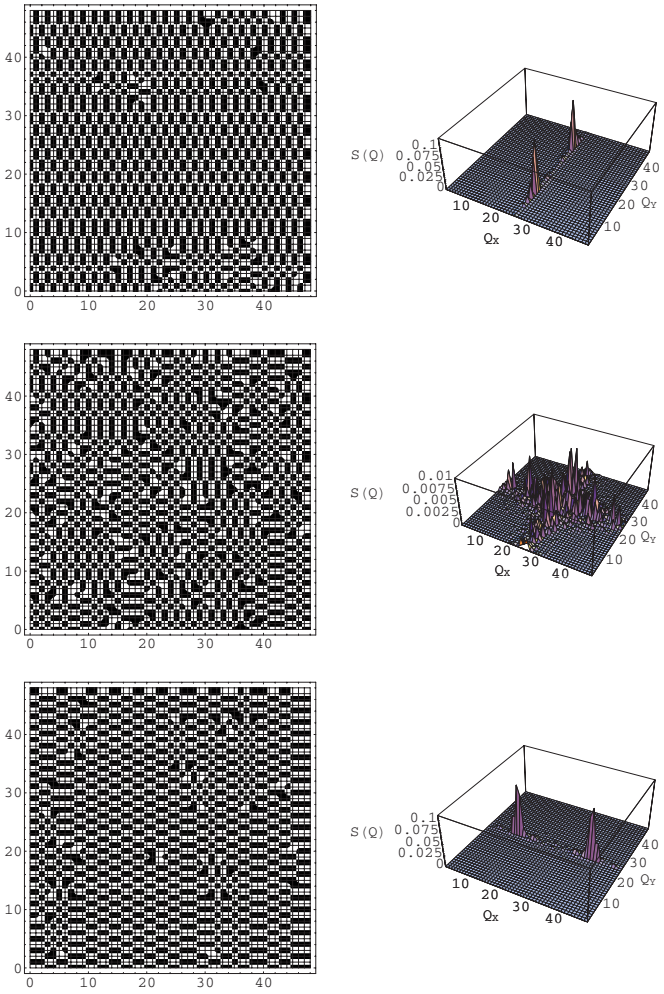

FIG. 5. (Color online) Snapshots and corresponding structure factors for $J/g=0.86$ and $k_BT/g=0.34$: $O_{hv}=0.301$, $E=-0.940$ (upper panel); $O_{hv}=0$, $E=-0.886$ (middle panel); $O_{hv}=-0.303$, $E=-0.931$ (lower panel).

The MC simulations around the boundary between the phases $\langle 2\rangle$ and $\langle 3\rangle$ lead to a different scenario. In Figs. 10 and 11, we show the specific heat, the order parameter, the energy, and order parameter density distribution together with two snapshots taken at the transition temperature for $J/g=4.3$ ($h=2$) and $J/g=4.4$ ($h=3$), respectively. For $J/g=4.3$, the specific heat shows three peaks: the first at $k_BT/g\simeq 1.42$, the second at $k_BT/g\simeq 1.48$, and the third at $k_BT/g\simeq 1.67$, as shown in Fig. 10(a). In correspondence to these temperatures, the order parameter shows three downward steps as shown in Fig. 10(b). The first two peaks of the specific heat, as well as the first two steps of the order parameter, are much more clean in each single run than in the average shown in Figs. 10(a) and 10(b) since they occur at slightly different temperatures going from one run to another. On the contrary, the third peak in the specific heat and the final fall of the order parameter are not changed passing from the single runs to the average.

A careful investigation of the structure factor $\langle S(\boldsymbol{Q})\rangle$ points out that the first peak in the specific heat and the first step in the order parameter correspond to a change of the order wave vector from $\boldsymbol{Q}=(0,\pm\pi/2)$ characterizing the "commensurate" (C) phase $\langle 2\rangle$ to an "incommensurate" (I) phase with $\boldsymbol{Q}=(0,\pm 11\pi/24)$. The second peak in the specific heat and the second step in the order parameter correspond to another change of the order wave vector from the value characterizing phase I to $\boldsymbol{Q}=(0,\pm 10\pi/24)$ characterizing a new incommensurate phase (I′). The peak intensity undergoes a discontinuous change from $\simeq 0.5$ (C phase) to $\simeq 0.3$ (I phase). No intensity change is observed at the transition between the two incommensurate phases I and I′, while a sudden intensity drop to $\simeq 0.1$ is seen at the transition between the incommensurate I′ phase and the tetragonal phase where the structure factor shows a four-peak pattern in which the peaks are located at $\boldsymbol{Q}=(0,\pm 10\pi/24)$ and $\boldsymbol{Q}=(\pm 10\pi/24,0)$. We call the incommensurate I and I′ phases *modulated phases*.

The energy and order parameter density distributions show a single δ-like peak for $k_BT/g<1.42$ corresponding to the ordered striped configuration $\langle 2\rangle$, a two-peak structure at $k_BT/g=1.42$ corresponding to the coexistence of the striped C and the modulated I phase, and a single-peak structure for $1.42<k_BT/g<1.48$ corresponding to the I phase. At $k_BT/g=1.48$, the two-peak structure points out the coexistence of the I and I′ phases. At $k_BT/g=1.49$, the single-peak structure corresponds to the I′ phase. The modulated-tetragonal transition is characterized by a broadening of the peak in $P(E)$ and by a two-peak structure in $P(O_{hv})$ near $k_BT/g\simeq 1.66$. Looking at the snapshots shown in Figs. 10(e) and 10(f) one can see that the modulated I phase can be thought as a combination of the phases $\langle 2\rangle$ and $\langle 3\rangle$, where the phase $\langle 2\rangle$ is predominant. The modulated I′ phase is an analogous combination in which, however, the phase $\langle 3\rangle$ is predominant and the presence of straits cutting the stripes is also noticed.

A similar scenario is obtained for $J/g=4.4$ ($h=3$), as shown in Fig. 11. A peak in the specific heat and a small step in the order parameter are found at $k_BT/g\simeq 1.52$. A broad peak in the specific heat and a drop of the order parameter are recorded around $k_BT/g\simeq 1.75$. This scenario is common to each single run. At $k_BT/g\simeq 1.52$, the structure factor shows a change from the commensurate C phase [with two main peaks at $\boldsymbol{Q}=(0,\pm\pi/3)$ and a secondary peak at $(0,\pi)$ corresponding to the phase $\langle 3\rangle$] to an incommensurate I phase with peaks at $\boldsymbol{Q}=(0,\pm 9\pi/24)$ corresponding to the modulated phase. No further change of the order wave vector was recorded.

A two-peak structure in $P(E)$ is seen only at $k_BT/g=1.52$, while the peak moves in a continuous way at increasing temperature. No clear two-peak structure is observed at the modulated-tetragonal transition: Only a broadening of the energy density distribution is found so that the modulated-tetragonal transition could be continuous or very weak first order. A two-peak structure is found at $k_BT/g=1.69$ in $P(O_{hv})$ corresponding to a free rotation of the stripes as it is expected in the tetragonal phase. From the snapshots, one can see the change from the striped phase $\langle 3\rangle$, stable at low temperature to the modulated phase stable at higher temperature. This phase is still a mixing of striped configurations $\langle 2\rangle$ and $\langle 3\rangle$. The transition to the tetragonal phase characterized by the appearance of a four-peak structure in $\langle S(\boldsymbol{Q})\rangle$ has been clearly seen at $k_BT/g=1.72$.

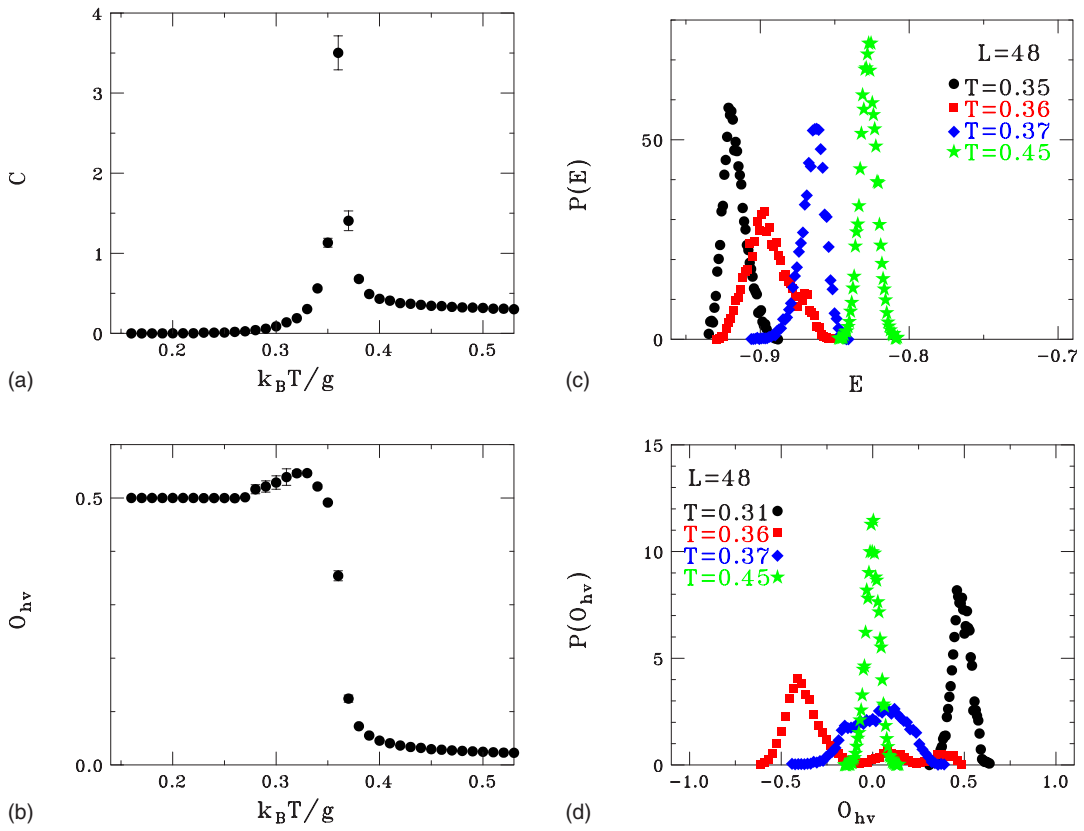

FIG. 6. (Color online) (a) Specific heat and (b) order parameter vs temperature for $J/g=0.88$ ($\langle 1,3\rangle$ phase); (c) energy density distribution $P(E)$ and (d) order parameter density distribution $P(O_{hv})$ for selected temperatures.

MC simulations around the boundary between the phases $\langle 3\rangle$ and $\langle 4\rangle$ have also been performed. The results for $J/g=5.6$ and 5.7 are shown in Figs. 12 and 13. For $J/g=5.6$, a weak peak at $k_BT/g\sim 2.1$ and a broad one at $k_BT/g\simeq 2.42$ in the specific heat are observed. The former is very sharp in each single run and occurs at temperature between 2.08 and 2.17 with a height varying between 0.54 and 0.89. The latter is more or less the same for each run. The same occurs for the order parameter: Each single run shows a step that becomes less sharp when the average is performed. The structure factor changes from the C phase with the main peaks at $\boldsymbol{Q}=(0,\pm\pi/3)$ to an incommensurate I phase with peaks at $\boldsymbol{Q}=(0,\pm 7\pi/24)$ in correspondence to the first peak of the specific heat and to the first step of the order parameter. In correspondence to the second peak of the specific heat, the structure factor assume a four-peak structure as a consequence of the free rotation of the stripes in the tetragonal phase.

The coexistence of the striped and modulated phases at $k_BT/g=2.10$ is confirmed by the double-peak structure of both the energy and order parameter density distribution [full (black) circles in Figs. 12(c) and 12(d)]. A single-peak structure in $P(E)$ is seen for $k_BT/g<2.10$ corresponding to the striped phase $\langle 3\rangle$. The same occurs for $2.11<k_BT/g<2.44$, where the peak moves toward higher energy. A two-peak structure at $k_BT/g=2.44$ points out the coexistence between the modulated and the tetragonal phase. A single peak for $k_BT/g>2.44$ corresponds to the disordered phase. The onset of the tetragonal phase is confirmed by the shape of the order parameter density distribution where two peaks are observed at $k_BT/g=2.40$ [(blue) diamonds of Fig. 12(d)], indicating a free rotation of the stripes. The snapshots at $k_BT/g=2.10$ show that the modulated phase consists of a mixing of striped phases $\langle 3\rangle$ and $\langle 4\rangle$.

MC simulations for $J/g=5.7$ support the scenario obtained for $J/g=5.6$ even though a jump in the specific heat replaces the peak observed for $J/g=5.6$ and the order parameter shows a small step upward instead of downward at the transition. The modulated phase is due to the coexistence of striped phases $\langle 3\rangle$ and $\langle 4\rangle$, as one can see in the snapshots at $k_BT/g=2.26$. The structure factor shows two main peaks at $\boldsymbol{Q}=(0,\pm\pi/4)$ characteristic of the striped phase $\langle 4\rangle$ for $k_BT/g<2.26$ and at $\boldsymbol{Q}=(0,\pm 7\pi/24)$ for $2.26<k_BT/g<2.38$ (modulated phase). A four-peak structure occurs for $k_BT/g>2.38$. The configuration of the modulated phase is similar to that found for $J/g=5.6$, so that it is not surprising that the plateau of O_{hv} is 0.8 high even for $J/g=5.7$. The phase coexistence cannot be detected in $P(E)$ and $P(O_{hv})$ because of the too small differences in energy $\Delta E\simeq 0.009$ and in order parameter $\Delta O_{hv}\simeq 0.015$ involved.

We have performed MC simulations also for $J/g=6,6.9,7,7.5,8.3,8.4$. The occurrence of a modulated phase is expected also near the phase boundary of larger striped phases, but the "quantization" of the order wave vector in a finite lattice makes it very difficult to single out such a phase. For instance, for $J/g=6.9$ and 7, we find that the structure

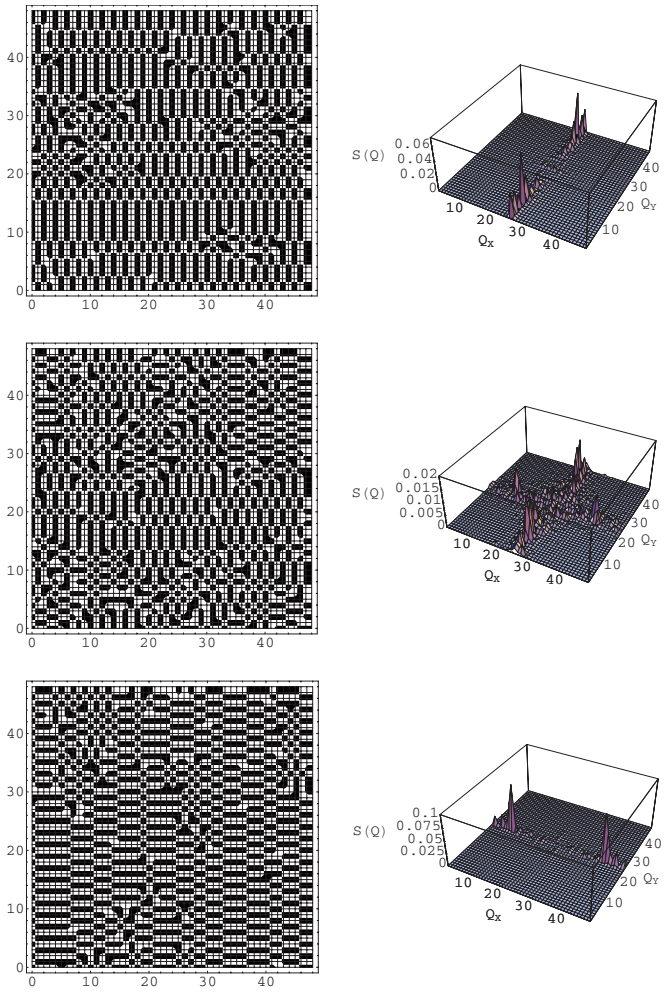

FIG. 7. (Color online) Snapshots and corresponding structure factors for $J/g=0.88$ and $k_BT/g=0.36$: $O_{hv}=0.403$, $E=-0.893$ (upper panel); $O_{hv}=0.101$, $E=-0.862$ (middle panel); $O_{hv}=-0.402$, $E=-0.895$ (lower panel).

factor shows peaks at the incommensurate wave vectors $\boldsymbol{Q}=(0,\pm 5\pi/24)$ until $k_BT/g\simeq 3.3$, where the tetragonal phase intervenes. This incommensurate phase meets the nonperiodic phase $\langle 4^2 5^8\rangle$ (discussed at the beginning of Sec. III) stable at $T=0$ for $6.63<J/g<7.23$. Between the striped phase $\langle 6\rangle$ $(J/g=8.3)$ characterized by an order wave vector $\boldsymbol{Q}=(0,\pm 4\pi/24)$ and the striped phase $\langle 8\rangle$ $(J/g=8.4)$ characterized by an order wave vector $\boldsymbol{Q}=(0,\pm 3\pi/24)$, peaks of the structure factor at an incommensurate wave vector $3\pi/24<Q_y<4\pi/24$ do not exist in a 48×48 lattice so that the modulated phase is undistinguishable from the commensurate $\langle 6\rangle$ or $\langle 8\rangle$ phase except for a reduced peak intensity owing to the mixing of the two stripe phases. Indeed, for $J/g=8.3$, we see a change in the location of the structure factor peak from $\boldsymbol{Q}=(0,\pm 4\pi/24)$ to $\boldsymbol{Q}=(0,\pm 3\pi/24)$ at $k_BT/g\simeq 3.70$ and we record the appearance of a four-peak structure (tetragonal phase) at $k_BT/g\simeq 4$. The peak intensity is about ~ 0.35 until this temperature. On the contrary, for $J/g=8.4$, we do not see any change in the order wave vector until $k_BT/g\simeq 4.13$ where the four-peak structure appears and the peak intensity drops from about 0.35 to about 0.2.

D. Ferromagnetic phase

For $J/g>17.27$, where the stable phase is the ferromagnetic one, a strange behavior of the specific heat vs temperature is found. In Fig. 14, where averages over eight independent runs are shown, a two-peak structure is clearly seen for $20<J/g<50$: The low temperature peak is very narrow while the high temperature peak is rather broad. For $60<J/g<100$, only one peak is seen. The shape of the first peak supports the existence of a first order phase transition between the ferromagnetic and the paramagnetic phase for $20<J/g<50$. For $J/g>50$, the narrow peak merges in the broad one. It is worthy of mentioning the features of the snapshots in the disordered phase for $J/g=20$ and 50. For $J/g=20$, the ferromagnetic order is destroyed at $k_BT/g\simeq 21$ via the onset of domains very similar to irregular stripes of large width $h\sim 24$. Notice that the regular striped phase stable at low temperature for $J/g<17.27$ is just the $\langle 24\rangle$ phase. For temperatures about the second peak of the specific heat $(k_BT/g\sim 30)$, the domains become similar to islands of size decreasing with temperature. For $J/g=50$, the ferromagnetic order is destroyed at $k_BT/g\simeq 90$ by a chaotic onset of islands of reversed spins similar to the domains seen in an Ising model with NN exchange interactions. The MC simulations seem to point out a change of the order of the phase transition around $J/g\simeq 50$.

We have performed a least squares fit of the transition temperature vs exchange interaction obtaining $k_BT_c=2.286J-(24.1\pm 0.3)g$. From the finite size correction to the critical temperature $k_BT_c(L)/J=2.269\,185+0.818/L$ and to the maximum of the specific heat $C_{max}(L)/(k_BL^2)=0.494\,538\,6\ln L+0.201\,359$ as given by Ferdinand and Fisher[12] for a square Ising model with NN exchange interaction, one has $k_BT_c(48)=2.286J$ and $C_{max}(48)/(k_B48^2)=2.116$. For $J/g=100$, we find that the specific heat maximum $C_{max}=2.11$ is undistinguishable from the result of Ferdinand and Fisher.[12] Notice that the reliability of our MC simulations is confirmed by the finite size scaling analysis for a square NN Ising model $(g=0)$, which gives $k_BT_c/J=2.269\pm 0.001+(0.76\pm 0.04)/L$ and $C_{max}/(k_BL^2)=(0.493\pm 0.008)\ln L+(0.20\pm 0.03)$ in very good agreement with the exact result of Ferdinand and Fisher.

The first order nature of the order-disorder transition may be supported by a self-consistent Hartree-Fock (SCHF) approximation applied to the continuous version of the Hamiltonian model.[2] The SCHF approximation was previously introduced for a model with an excitation energy spectrum showing a rotonlike minimum[13] and subsequently applied to a three-dimensional (3D) Ising model with ferromagnetic NN coupling and long range Coulomb interaction.[14] However, this approach is not conclusive because, for the present model, a first order phase transition is found for any value of the dipole interaction g, including $g=0$ as shown in Appendix B. For $g=0$, the model reduces to the square NN Ising model for which the transition is continuous. The conclusion could be that the fluctuations accounted for by the SCHF approximation always drive the transition to first order.

IV. PHASE DIAGRAM

In Fig. 15, we sketch the phase diagram as obtained from analytic calculations at $T=0$ and MC simulations on a 48

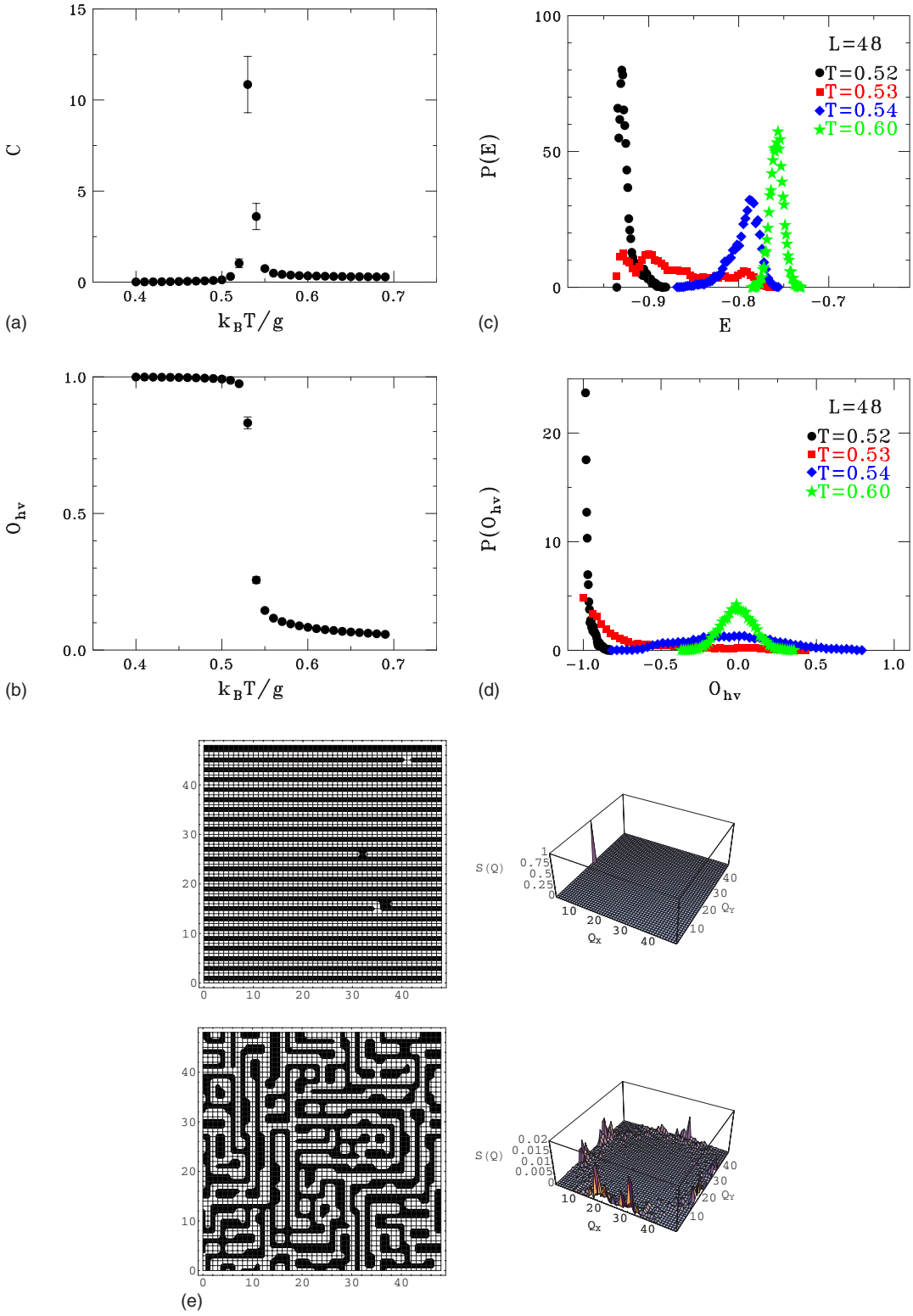

FIG. 8. (Color online) The same as Figs. 6 and 7 for $J/g=2.5$ ($h=1$); the snapshots are taken at $k_BT/g=0.53$: $O_{hv}=-0.993$, $E=-0.930$ (upper panel); $O_{hv}=0.022$, $E=-0.780$ (lower panel).

$\times 48$ lattice at finite temperature. A careful investigation was focused on values of J/g about the phase boundaries between the striped configurations $\langle 1\rangle-\langle 2\rangle$, $\langle 2\rangle-\langle 3\rangle$, and $\langle 3\rangle-\langle 4\rangle$. The transition to the disordered phase is shown by the continuous (black) line in Fig. 15. As one can see the phase diagram shows a variety of configurations depending on the ratio J/g. Indeed, for $J=0$ (pure dipole interaction), the ground state corresponds to an antiferromagnetic Néel (N) configuration. As the ratio J/g increases, the ground state is characterized by $\langle 1,n\rangle$ configurations in the narrow range

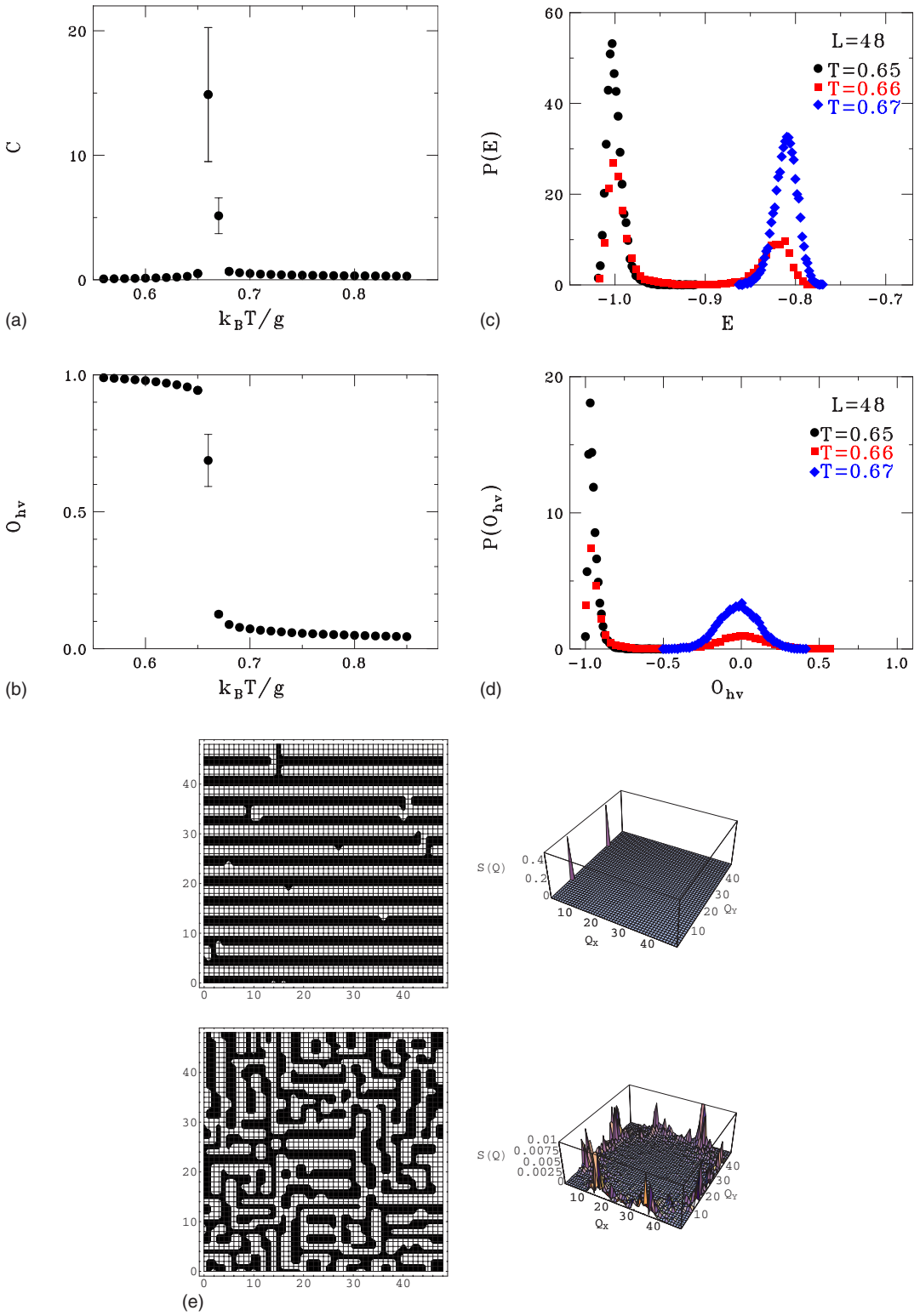

FIG. 9. (Color online) The same as Fig. 8 for $J/g=2.6$ ($h=2$); the snapshots are taken at $k_BT/g=0.66$: $O_{hv}=-0.906$, $E=-0.993$ (upper panel); $O_{hv}=0.011$, $E=-0.815$ (lower panel).

0.8304–0.8806 and by striped configurations $\langle h\rangle$ with $h=1,2,3,4,6,8,12,24$ (the last two not shown in the phase diagram) for $0.8806<J/g<17.27$. For $6.63<J/g<7.23$, a nonperiodic spin configuration we call $\langle\sim 5\rangle$ consisting of two stripes of width 4 and eight stripes of width 5 is found. It is clear that this result is an artifact of the finite size of the lattice ($L=48$). Indeed in the thermodynamic limit, only regular periodic stripe configurations are allowed. Finally, for $J/g>17.27$, the ferromagnetic configuration becomes stable.

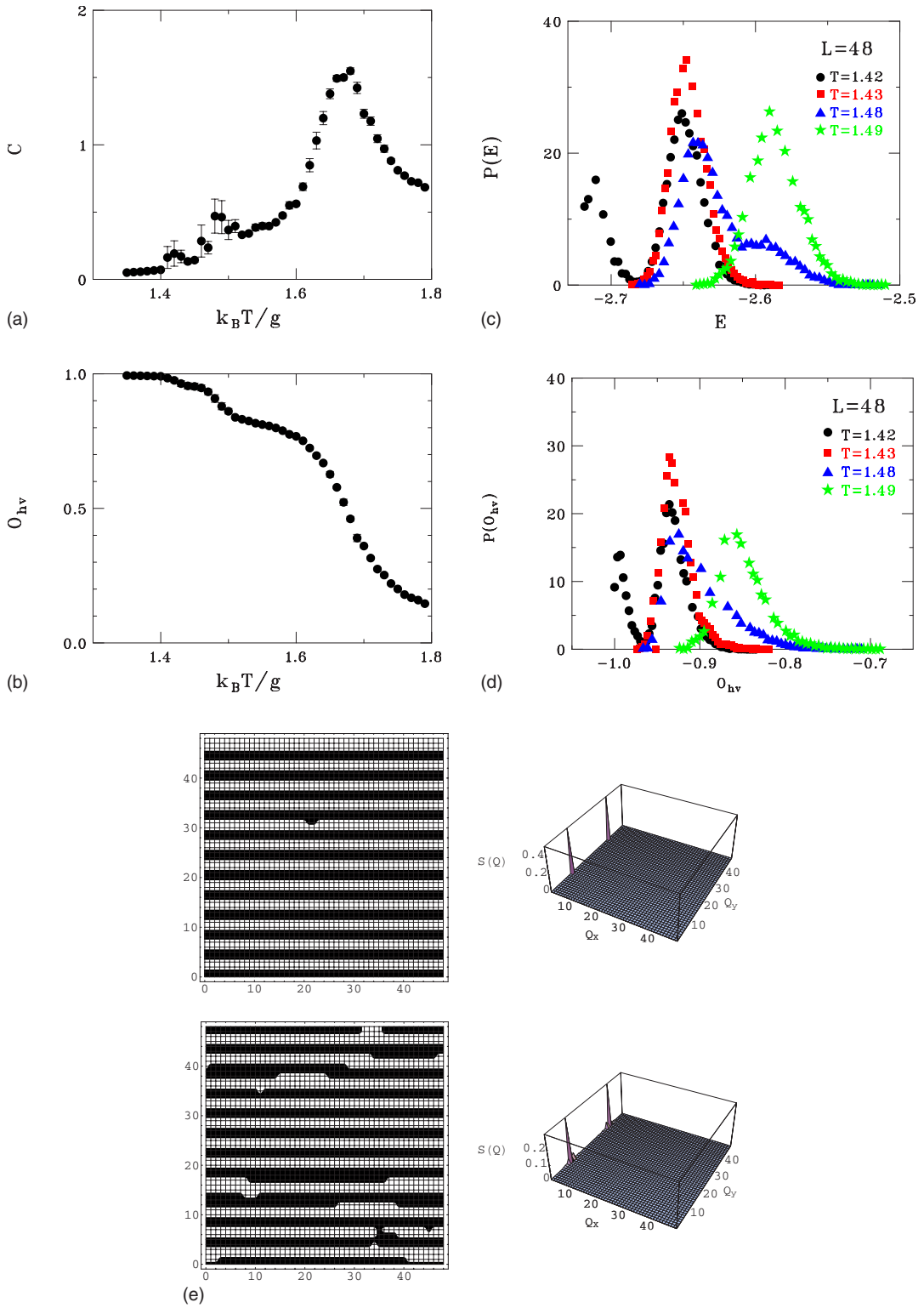

FIG. 10. (Color online) The same as Fig. 8 for $J/g=4.3$ ($h=2$); the snapshots are taken at $k_BT/g=1.42$: $O_{hv}=-0.997$, $E=-2.713$ (upper panel); $O_{hv}=-0.952$, $E=-2.655$ (lower panel).

The phase diagram of Fig. 15 has to be compared with the phase diagram shown in Fig. 6 of MacIsaac *et al.*[6] Some of the striped configurations shown in Fig. 15 are missing in Fig. 6 of MacIsaac *et al.*[6] because of the reduced size of their lattice (16×16). An important difference between our phase diagram and Fig. 6 of MacIsaac *et al.*[6] is the existence of a modulated phase in the proximity of the phase boundaries $\langle2\rangle-\langle3\rangle$ and $\langle3\rangle-\langle4\rangle$. We confirm the disappearance of the modulated phase far from the boundaries and near the boundary $\langle1\rangle-\langle2\rangle$. We confirm the continuous nature of the

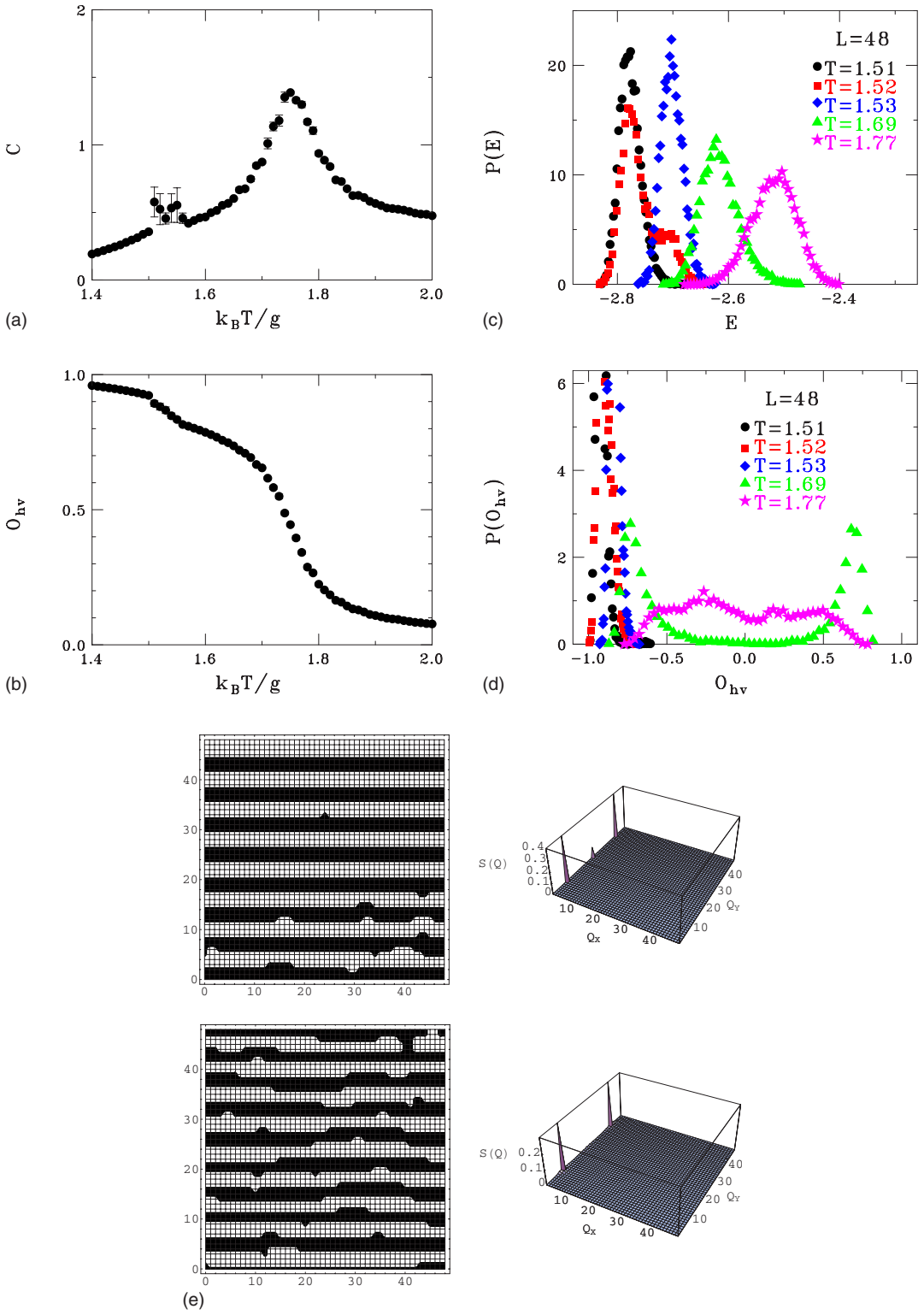

FIG. 11. (Color online) The same as Fig. 8 for $J/g=4.4$ ($h=3$); the snapshots are taken at $k_BT/g=1.52$: $O_{hv}=-0.935$, $E=-2.783$ (upper panel); $O_{hv}=-0.845$, $E=-2.701$ (lower panel).

transition for small J/g where the ground state configuration is a Néel state. We found[4] that for $J=0$, the critical exponents are those of the NN Ising model. For $0<J/g<0.8$, the specific heat vs temperature is very similar to that obtained for $J=0$. A continuous transition occurs at a temperature decreasing linearly from $k_BT/g=2.38$ to 0.36 as J/g goes from 0 to 0.8. On the contrary, in the narrow region $0.83<J/g<0.88$, the specific heat shows a sharp peak typical of a first order phase transition so that a tricritical point is expected to occur. The transition to the disordered phase appears to be first order for the striped phases $\langle h\rangle$ with $h>1$. Around the boundaries between the striped configurations $\langle 2\rangle-\langle 3\rangle$ and

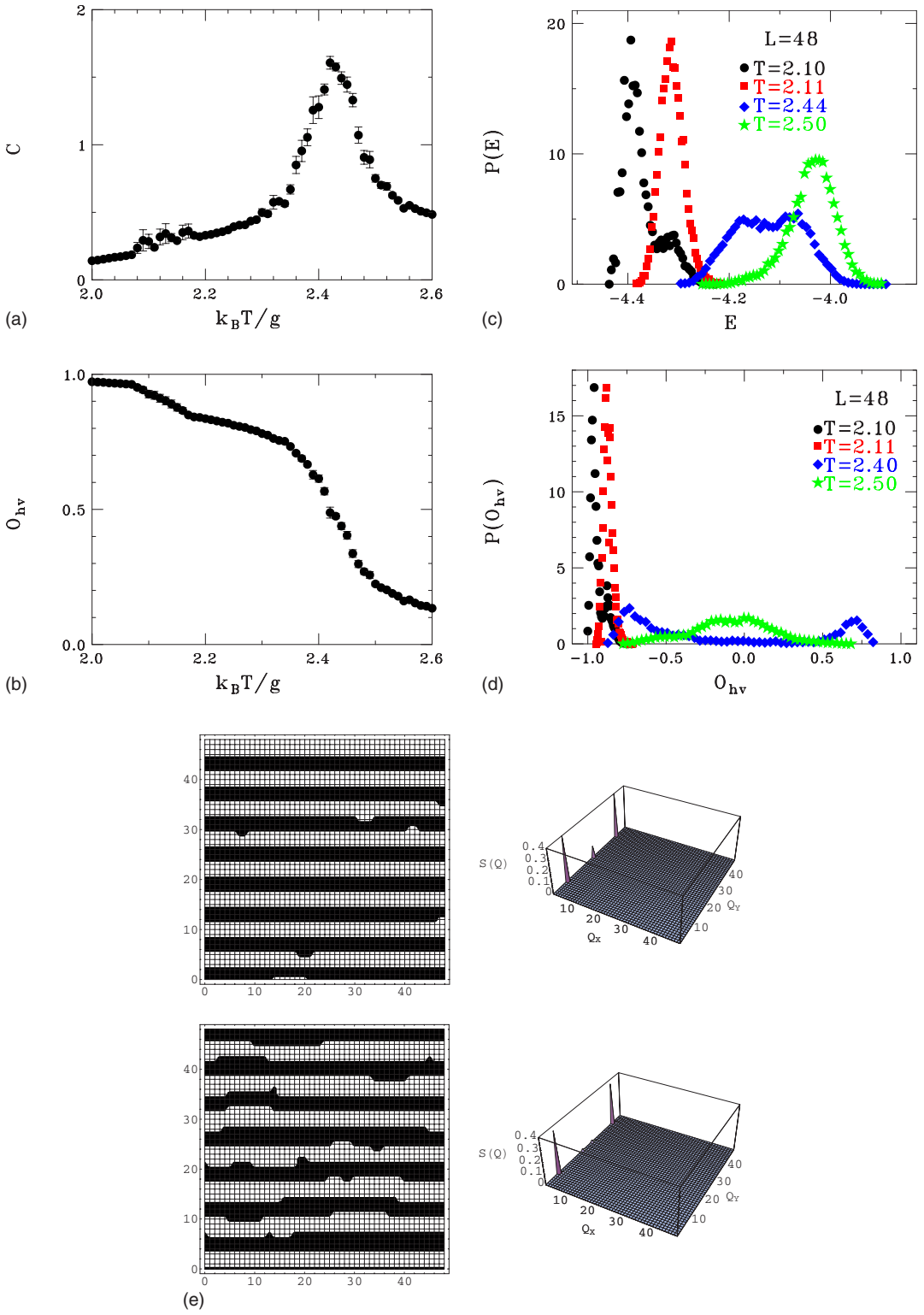

FIG. 12. (Color online) The same as Fig. 8 for $J/g=5.6$ ($h=3$); the snapshots are taken at $k_BT/g=2.10$: $O_{hv}=-0.964$, $E=-4.391$ (upper panel); $O_{hv}=0.888$, $E=-4.325$ (lower panel).

$\langle 3\rangle-\langle 4\rangle$, a modulated phase characterized by a $\boldsymbol{Q}$ wave vector incommensurate with the underlying lattice occurs between the striped phase and the paramagnetic one. The transition between the striped and modulated phases is represented by a continuous red (gray) line in Fig. 15. The phase diagram of Fig. 15 is similar to that shown in Fig. 2 of Grousson *et al.*[15] who studied a three-dimensional Ising model with nearest neighbor ferromagnetic exchange interaction J and long range Coulomb interaction Q by MC simulations on cubic lattices of sides between $L=4$ and $L=16$.

In summary, continuous order-disorder phase transition is confirmed for the N phase. A first order phase transition

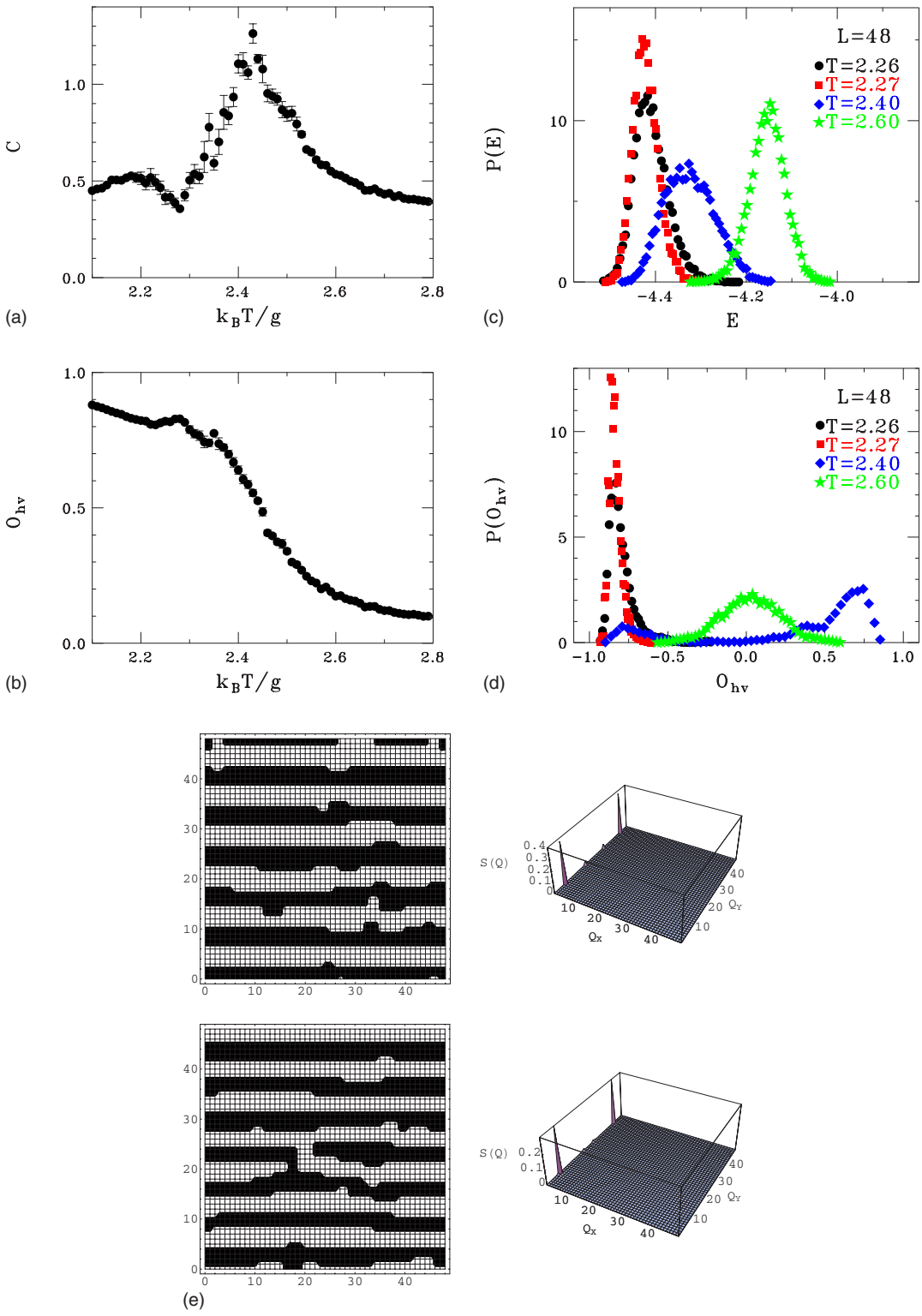

FIG. 13. (Color online) The same as Fig. 8 for $J/g=5.7$ ($h=4$); the snapshots are taken at $k_BT/g=2.26$: $O_{hv}=-0.829$, $E=-4.443$ (upper panel); $O_{hv}=-0.844$, $E=-4.434$ (lower panel).

seems to occur for $\langle 1,n\rangle$ phases. As for the $\langle 1\rangle$ phase, the order-disorder phase transition appears to be first order near the boundaries with the $\langle 1,n\rangle$ and the $\langle 2\rangle$ phases, while for $J/g=1.7$, the phase transition seems to be continuous with nonuniversal critical exponents.[4] A clear first order transition was found between the striped phase $\langle 2\rangle$ (Refs. 2 and 4) and the tetragonal phase, while for the striped phase $\langle 3\rangle$, the transition appears to be weakly first order. For $h=4$, any conclusion about the nature of the transition is hard since the simulations are compatible with a continuous transition, but a very weak first order transition cannot be ruled out. To get reliable information for larger striped phases, larger lattice

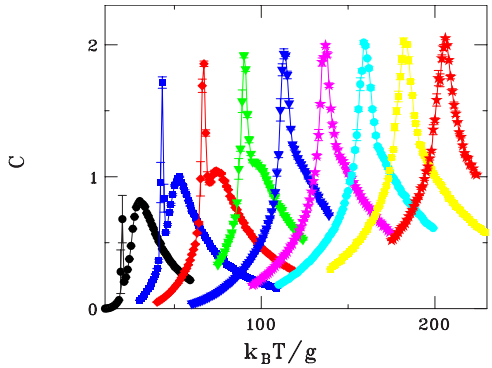

FIG. 14. (Color online) Specific heat vs temperature for several J/g. From left to right, $J/g=20,30,40,50,60,70,80,90,100$.

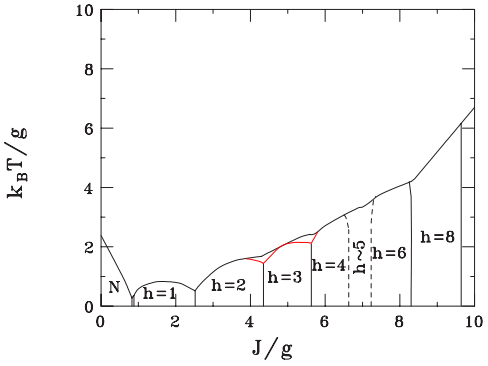

FIG. 15. (Color online) Phase diagram of a square lattice with $L=48$. The region between the red (gray) and black line is the region where the modulated phase is expected to occur.

sizes should have to be investigated, but the computer time increases as L^4, where L is the lattice side owing to the long range nature of the dipole interaction.

V. CONCLUSIONS

The Ising model with NN ferromagnetic exchange and dipole interaction provides a comprehensive survey of possible behaviors in the phase transitions. Indeed, first order and continuous transitions, tricritical points, and modulated phases between striped (smectic) and paramagnetic (tetragonal) phases are found by MC simulation at finite temperature. A very rich phase diagram $(J/g, k_BT/g)$ is shown in Fig. 15. At $T=0$, an analytic calculation led to the discovery of another class of checkerboard configurations $<1,n>$ in a narrow region of J/g located between the Néel (N) and the columnar phase. MC simulations at finite T confirm the existence of these checkerboard phases. The model studied here shows a phase diagram even richer than that found for the well known and widely studied ANNNI model.[9] Like the ANNNI model, the present model shows a "multiphase point" at $J/g=0.88$, $T=0$. Moreover, at low temperature, a sequence of striped phases is found increasing J/g, while the ordered phases of the ANNNI model were restricted to the ferromagnetic (F) and the $\langle 2\rangle$ phase (antiphase). At intermediate temperature, the present model supports the existence of a modulated phase restricted to the region between the striped phases with $h=2,3,4$. This phase is like the floating phase of the ANNNI model. Like the ANNNI model,[16] where the Lifshitz point on the ferromagnetic side of the phase diagram is seen to disappear as the size increases, in the present model, the location of the multicritical point in the ferromagnetic region could be affected by the finite size even though its occurrence is certain.

APPENDIX A: $\langle h_1, h_2\rangle$ PHASES

Assume a double periodic spin configuration with period $p_1=2h_1$ along the x axis and $p_2=2h_2$ along the y axis of a square lattice of size L, with L supposed to be an even number. Label each lattice site by a couple of integer numbers n,m with $n,m=1,\ldots,L$. The periodicity implies that the spin at site (m,n) $\sigma_{m,n}$ is the same as the spin at site $m+s_1p_1, n+s_2p_2$, with $s_1=0,1,\ldots,L/p_1-1$ and $s_2=0,1,\ldots,L/p_2-1$. The finite Fourier transform of the spin is

$$\sigma_{\mathbf{Q}} = \frac{1}{L}\sum_{m=1}^{L}\sum_{n=1}^{L}\sigma_{m,n}e^{-i(2\pi/L)q_1m}e^{-i(2\pi/L)q_2n}$$
$$= \frac{1}{L}\sum_{m=1}^{p_1}\sum_{n=1}^{p_2}\sigma_{m,n}e^{-i(2\pi/L)q_1m}e^{-i(2\pi/L)q_2n}\sum_{s_1=0}^{L/p_1-1}\sum_{s_2=1}^{L/p_2-1}$$
$$\times e^{-i(2\pi/L)s_1p_1}e^{-i(2\pi/L)s_2p_2}. \tag{A1}$$

Using the relationship

$$\sum_{s_1=0}^{L/p_1-1} e^{-i(2\pi/L)s_1p_1} = \frac{L}{p_1}g_1\delta\left(q_1,\frac{L}{p_1}g_1\right), \tag{A2}$$

where $g_1=0,1,\ldots,p_1-1$, one obtains

$$\sigma_{\mathbf{Q}} = \frac{L}{p_1p_2}\delta\left(q_1,\frac{L}{p_1}g_1\right)\delta\left(q_2,\frac{L}{p_2}g_2\right)\sum_{m=1}^{p_1}\sum_{n=1}^{p_2}\sigma_{m,n}e^{-i(2\pi/L)q_1m}e^{-i(2\pi/L)q_2n} = (1-e^{-i(2\pi/L)q_1h_1})(1$$
$$-e^{-i(2\pi/L)q_2h_2})\sum_{m=1}^{h_1}e^{-i(2\pi/L)q_1m}\sum_{n=1}^{h_2}e^{-i(2\pi/L)q_2n}. \tag{A3}$$

From the identity

$$(1-e^{-i(2\pi/L)q_1h_1})\sum_{m=1}^{h_1} e^{-i(2\pi/L)q_1m} = 2e^{-i(\pi/h_1)(2s_1+1)}\frac{1-e^{-i\pi(2s_1+1)}}{1-e^{-i(\pi/h_1)(2s_1+1)}}, \tag{A4}$$

with $s_1=0,1,\ldots,h_1-1$, one obtains

$$\sigma_{\mathbf{Q}} = \frac{L}{h_1h_2}\delta\left(\frac{q_1}{L},\frac{s_1+\frac{1}{2}}{h_1}\right)\delta\left(\frac{q_2}{L},\frac{s_2+\frac{1}{2}}{h_2}\right)(1-e^{-i\pi(2s_1+1)})(1-e^{-i\pi(2s_2+1)})\frac{e^{-i(\pi/h_1)(2s_1+1)}}{1-e^{-i(\pi/h_1)(2s_1+1)}}\frac{e^{-i(\pi/h_2)(2s_2+1)}}{1-e^{-i(\pi/h_2)(2s_2+1)}}, \tag{A5}$$

with $s_1=1,2,\ldots,h_1-1$ and $s_2=1,1,2,\ldots,h_2$. It is easy to obtain

$$|\sigma_{\mathbf{Q}}|^2 = L^2\delta\left(\frac{q_1}{L},\frac{s_1+\frac{1}{2}}{h_1}\right)\delta\left(\frac{q_2}{L},\frac{s_2+\frac{1}{2}}{h_2}\right)\frac{1}{h_1^2h_2^2\sin^2\left[\frac{\pi}{h_1}\left(s_1+\frac{1}{2}\right)\right]\sin^2\left[\frac{\pi}{h_2}\left(s_2+\frac{1}{2}\right)\right]}. \tag{A6}$$

The zero temperature energy becomes

$$E_{\langle h_1,h_2\rangle} = \sum_{\mathbf{Q}}\left[-J\left(\cos\frac{2\pi}{L}q_1+\cos\frac{2\pi}{L}q_2\right)+gD^{zz}\left(\frac{2\pi}{L}q_1,\frac{2\pi}{L}q_2\right)\right]|\sigma_{\mathbf{Q}}|^2 = \frac{L^2}{h_1^2h_2^2}\sum_{s_1=0}^{h_1-1}\sum_{s_2=0}^{h_2-1}\left\{-J\left[\cos\frac{2\pi}{h_1}\left(s_1+\frac{1}{2}\right)\right.\right.$$
$$\left.\left.+\cos\frac{2\pi}{h_2}\left(s_2+\frac{1}{2}\right)\right]+gD^{zz}\left[\frac{2\pi}{h_1}\left(s_1+\frac{1}{2}\right),\frac{2\pi}{h_1}\left(s_2+\frac{1}{2}\right)\right]\right\}\frac{1}{\sin^2\left[\frac{\pi}{h_1}\left(s_1+\frac{1}{2}\right)\right]\sin^2\left[\frac{\pi}{h_2}\left(s_2+\frac{1}{2}\right)\right]}, \tag{A7}$$

where

$$D^{zz}(\mathbf{Q}) = \sum_{r\neq 0}\frac{e^{i\mathbf{Q}\cdot\mathbf{r}}}{r^3}. \tag{A8}$$

From the equations

$$\sum_{s=0}^{h-1}\frac{1}{h^2\sin^2\left[\frac{\pi}{h}\left(s+\frac{1}{2}\right)\right]} = 1, \tag{A9}$$

$$\sum_{s=0}^{h-1}\frac{\cos\left[\frac{\pi}{h}(2s+1)\right]}{h^2\sin^2\left[\frac{\pi}{h}\left(s+\frac{1}{2}\right)\right]} = 1-\frac{2}{h}, \tag{A10}$$

we have

$$\frac{E_{\langle h_1,h_2\rangle}}{gL^2} = -2\frac{J}{g}\left(1-\frac{1}{h_1}-\frac{1}{h_2}\right) + \sum_{s_1=0}^{h_1-1}\sum_{s_2=0}^{h_2-1}\frac{D^{zz}\left[\frac{2\pi}{h_1}\left(s_1+\frac{1}{2}\right),\frac{2\pi}{h_2}\left(s_2+\frac{1}{2}\right)\right]}{h_1^2h_2^2\sin^2\left[\frac{\pi}{h_1}\left(s_1+\frac{1}{2}\right)\right]\sin^2\left[\frac{\pi}{h_2}\left(s_2+\frac{1}{2}\right)\right]}. \tag{A11}$$

The zero temperature energy of the striped configurations $\langle h,\infty\rangle$ (vertical stripes) or $\langle\infty,h\rangle$ (horizontal stripes) becomes

$$\frac{E_{\langle h\rangle}}{gL^2} = -2\frac{J}{g}\left(1-\frac{1}{h}\right)+\frac{1}{h^2}\sum_{s=0}^{h-1}\frac{D^{zz}\left[\frac{2\pi}{h}\left(s+\frac{1}{2}\right),0\right]}{\sin^2\left[\frac{\pi}{h}\left(s+\frac{1}{2}\right)\right]}. \tag{A12}$$

Finally, the zero temperature energy of the ferromagnetic configuration is given by

$$\frac{E_F}{gL^2} = -2\frac{J}{g}+D^{zz}(0,0), \tag{A13}$$

where $D^{zz}(0,0)=9.033\,621\,683\,1$. Because of the symmetry of the Fourier transform of the dipolar interaction $D^{zz}(Q,0)=D^{zz}(2\pi-Q,0)$, the sum in Eq. (A12) can be restricted to $(h-1)/2$ subtracting the term $D^{zz}(\pi,0)/h^2$ with $D^{zz}(\pi,0)=-0.935\,462\,154\,6$ when h is odd, to avoid a double counting of that term. For stripes of large width $(h\to\infty)$, one can expand $D^{zz}(Q,0)$ for $Q\to 0$ retaining only linear and quadratic terms in the wave vector,

$$D^{zz}(Q,0) = 9.033\,621\,683\,1-2\pi Q+0.975\,066\,230\,0Q^2. \tag{A14}$$

Replacing expansion (A14) into Eq. (A12), one obtains

$$\frac{E_{\langle h\rangle}(h\to\infty)}{gL^2} = -2\frac{J}{g}\left(1-\frac{1}{h}\right)+9.033\,621\,683-\frac{8}{h}\ln h - \frac{9.143\,325\,854}{h}+O\left(\frac{1}{h^2}\right), \tag{A15}$$

where use of the following relationships has been done:

$$\frac{2}{h^2}\sum_{s=0}^{(h-1)/2}\frac{1}{\sin^2\left[\frac{\pi}{h}\left(s+\frac{1}{2}\right)\right]}=1, \tag{A16}$$

$$\frac{4\pi}{h^3}\sum_{s=0}^{(h-1)/2}\frac{\left(s+\frac{1}{2}\right)}{\sin^2\left[\frac{\pi}{h}\left(s+\frac{1}{2}\right)\right]}=\frac{4}{\pi h}\ln h+\frac{2.315\,742\,797}{h}+O\left(\frac{1}{h^2}\right), \tag{A17}$$

$$\frac{8\pi^2}{h^4}\sum_{s=0}^{(h-1)/2}\frac{\left(s+\frac{1}{2}\right)^2}{\sin^2\left[\frac{\pi}{h}\left(s+\frac{1}{2}\right)\right]}=\frac{5.545\,177\,445}{h}+O\left(\frac{1}{h^2}\right). \tag{A18}$$

Equation (A16) is exact, while Eqs. (A17) and (A18) are obtained by an expansion in $1/h$ retaining only terms proportional to $1/h$. These expansions are in good agreement with those reported by MacIsaac *et al.*[6] The small differences between our coefficients of the terms proportional to $1/h$ and those of MacIsaac *et al.*[6] come from their treatment of the sum over k in Eqs. (B37) and (B39) where terms of order $1/h$ have been neglected.

The zero temperature energy of the $\langle 1,n\rangle$ phases is given by

$$\frac{E_{\langle 1,n\rangle}}{gL^2}=\frac{2}{n}\frac{J}{g}+\frac{1}{n^2}\sum_{s=0}^{n-1}\frac{D^{zz}\left[\pi,\frac{2\pi}{n}\left(s+\frac{1}{2}\right)\right]}{\sin^2\left[\frac{\pi}{n}\left(s+\frac{1}{2}\right)\right]}. \tag{A19}$$

For $n\to\infty$, one can expand $D^{zz}(\pi,Q)$ for $Q\to 0$ retaining only quadratic terms in Q,

$$D^{zz}(\pi,Q)=-0.935\,462\,154\,6-0.317\,618\,140Q^2. \tag{A20}$$

At variance with the expansion around $\boldsymbol{Q}=(0,0)$, the expansion around $\boldsymbol{Q}=(\pi,0)$ does not contain linear terms. This implies that the energy of the $\langle 1,n\rangle$ phase does not contain logarithmic terms. Indeed, one has

$$\frac{E_{\langle 1,n\rangle}(n\to\infty)}{gL^2}=\frac{2}{n}\frac{J}{g}-0.935\,462\,154\,6-\frac{1.761\,248\,944}{n}+O\left(\frac{1}{n^2}\right), \tag{A21}$$

where use of Eqs. (A16) and (A18) has been done.

APPENDIX B: SELF-CONSISTENT HARTREE APPROXIMATION

The field theoretical version of the two-dimensional Ising model with exchange and dipole interaction corresponds to the Hamiltonian[2]

$$\mathcal{H}[\{\phi_k\}]=\frac{1}{2}\sum_k A(k)\phi_k\phi_{-k}+\frac{1}{4}u\sum_{k_1,k_2,k_3}\phi_{k_1}\phi_{k_2}\phi_{k_3}\phi_{-k_1-k_2-k_3}, \tag{B1}$$

where (assuming the exchange integral to be $J=1$)

$$A(k)=r_0+k^2+2g(-2\pi k+0.975\,066k^2)=r_0'+(1+1.950\,13g)(k-k_0)^2\simeq r_0+(k-k_0)^2, \tag{B2}$$

with $r_0'=r_0-(2\pi g)^2/(1+1.950\,13g)\simeq r_0\equiv(T-T_{MF})$, where $T_{MF}=4$ is the critical temperature (in units of J/k_B) of the mean field approximation and $k_0=(2\pi g)/(1+1.950\,13g)\simeq 2\pi g$. We assume that $g\ll 1$ where the long wavelength limit holds. Equation (B2) is obtained from the small-k expansion of both the exchange and dipole interaction [see Eq. (A14)]. Analogous equations were obtained by Grousson *et al.*[14] for a 3D Ising model with Coulomb interaction and by Cannas *et al.*[2] for the present model. The spectrum of Eq. (B2) may also be compared to the rotonlike excitation spectrum of the model studied by Brazovskii.[13] According to Grousson *et al.*,[14] we assume the field ϕ_k to be the sum of an average component $m_k=\langle\phi_k\rangle$ such that $m_k=m(\delta_{k,k_0}+\delta_{k,-k_0})$ and a fluctuation $\psi_k=\phi_k-m_k$. The field Hamiltonian [Eq. (B1)] reduces to

$$\mathcal{H}[\{\psi_k\},m]=r_0m^2+\frac{3}{2}um^4+\frac{1}{2}\sum_k[A(k)+6um^2]\psi_k\psi_{-k}+\frac{1}{4}u\sum_{k_1,k_2,k_3}\psi_{k_1}\psi_{k_2}\psi_{k_3}\psi_{-k_1-k_2-k_3}. \tag{B3}$$

The Peierls' variational theorem states

$$\mathcal{F}\leqslant\mathcal{F}_0+\langle\mathcal{H}-\mathcal{H}_0\rangle_0, \tag{B4}$$

where $\mathcal{F}$ is the free energy of the model, $\mathcal{F}_0$ is the free energy of an arbitrary trial Hamiltonian, and the average $\langle\cdots\rangle_0$ means the average over the density matrix of the trial Hamiltonian. We choose as trial Hamiltonian

$$\mathcal{H}_0=\frac{1}{2}\sum_k\epsilon_k\psi_k\psi_{-k}, \tag{B5}$$

so that the average $\langle\psi_k\psi_{-k}\rangle_0$ is easily performed leading to

$$\langle\psi_k\psi_{-k}\rangle_0=\frac{T}{\epsilon_k}. \tag{B6}$$

Minimization of Eq. (B4) with respect to the variational parameter ϵ_k leads to the self-consistent equation

$$\epsilon_k=A(k)+6um^2+3uT\sum_k\frac{1}{\epsilon_k}. \tag{B7}$$

Putting $\epsilon_k=r+(k-k_0)^2$, a self-consistent equation for r is obtained,

$$r = r_0 + 3uT\sum_{\boldsymbol{k}} \frac{1}{r + (k - k_0)^2}. \tag{B8}$$

Minimization of Eq. (B4) with respect to the other variational parameter m leads to the equation

$$m\left(r_0 + 3um^2 + 3uT\sum_{\boldsymbol{k}} \frac{1}{\epsilon_{\boldsymbol{k}}} \right) = 0. \tag{B9}$$

Note that Eqs. (B8) and (B9) coincide with those found by Brazovskii,[13] Grousson *et al.*,[14] and Cannas *et al.*[2] The solutions of these equations are

$$m = 0, \quad r = r_0 + 3uT\sum_{\boldsymbol{k}} \frac{1}{r + (k - k_0)^2},$$

$$\mathcal{F}_{dis} = -\frac{1}{2}T\ln T + \frac{1}{2}\sum_{\boldsymbol{k}} \ln[r + (k - k_0)^2] - \frac{1}{12}\frac{(r - r_0)^2}{u}, \tag{B10}$$

for the disordered phase, and

$$m = \sqrt{\frac{r}{3u}}, \quad r = -r_0 - 3uT\sum_{\boldsymbol{k}} \frac{1}{r + (k - k_0)^2},$$

$$\mathcal{F}_{ord} = -\frac{1}{2}T\ln T + \frac{1}{2}\sum_{\boldsymbol{k}} \ln[r + (k - k_0)^2] - \frac{1}{12}\frac{(r + r_0)^2}{u} + \frac{1}{6}\frac{r(r + 2r_0)}{u}, \tag{B11}$$

for the ordered phase. Now, we evaluate the sums in Eqs. (B10) and (B11) assuming the cutoff wave vector to be 1. Then,

$$\sum_{\boldsymbol{k}} \frac{1}{r + (k - k_0)^2} \simeq \frac{1}{(2\pi)}\int_0^1 kdk \frac{1}{r + (k - k_0)^2} = \frac{1}{(4\pi)}\left[\ln\frac{r + (1 - k_0)^2}{r + k_0^2} + \frac{2k_0}{\sqrt{r}} \times \left(\arctan\frac{1 - k_0}{\sqrt{r}} + \arctan\frac{k_0}{\sqrt{r}} \right) \right], \tag{B12}$$

$$\sum_{\boldsymbol{k}} \ln[r + (k - k_0)^2] \simeq \frac{1}{(2\pi)}\int_0^1 kdk \ln[r + (k - k_0)^2] = \frac{1}{(4\pi)}\left\{ r\ln\frac{r + (1 - k_0)^2}{r + k_0^2} + 2k_0\sqrt{r}\left(\arctan\frac{1 - k_0}{\sqrt{r}} + \arctan\frac{k_0}{\sqrt{r}} \right) + (1 - k_0)\ln[r + (1 - k_0)^2] + 1 - 4k_0 \right\}. \tag{B13}$$

The value of these integrals differs from that obtained by Brazovskii[13] because of two reasons: a different space dimensionality (2 in the present case, 3 in the model studied by Brazovskii) and a different assumption about the value of k_0 (the rotonlike model of Brazovskii assumes that $k_0 \gg 1$, whereas we assume $k_0 \ll 1$ since we look at the limit $g \ll 1$). Assuming $k_0 \gg 1$, our results reduce to those of Brazovskii. On the contrary, if we assume $k_0 \ll 1$, the logarithmic terms of Eqs. (B12) and (B13), neglected by Brazovskii, become crucial. Notice that in the limit $k_0 \to 0$ (two-dimensional NN exchange Ising model), one obtains for the disordered phase

$$m = 0, \quad r = r_0 + \ln\frac{r + 1}{r},$$

$$6u\mathcal{F}_{dis} = f + \ln(1 + r) + \frac{1}{2}(r^2 - r_0^2), \tag{B14}$$

where f is a free energy contribution independent of r. We have assumed for simplicity that $3uT/(4\pi) = 1$. The self-consistent equation for r has one solution for any r_0. For the ordered phase, one has

$$m = \sqrt{\frac{r}{3u}}, \quad r = -r_0 - \ln\frac{r + 1}{r},$$

$$6u\mathcal{F}_{ord} = f + \ln(1 + r) - \frac{1}{2}(r^2 + r_0^2). \tag{B15}$$

The self-consistent equation for r has two solutions r_1, r_2 only for $r_0 < r_0^* = -1.5804$. The two solutions meet for $r_0 = r_0^*$ $(r_1 = r_2 = 0.618)$ and disappear for $r_0 > r_0^*$. One can see that for $r_1 < r_2$, the corresponding free energies are $\mathcal{F}_{ord}(r_1) > \mathcal{F}_{ord}(r_2)$, so that the solution corresponding to r_1 is always unstable. Comparing the free energy of the ordered phase $\mathcal{F}_{ord}(r_2)$ with that of the disordered phase $\mathcal{F}_{dis}(r)$, one finds that for $r_0^* > r_0 > r_0^t = -1.7054$, the stable phase is the disordered one, whereas for $r_0 < r_0^t$, the stable phase is the ordered one. At the transition r_0^t, corresponding to $T_t = 2.2945$, the order parameter jumps from $m_t = \sqrt{r_2/(3u)}$ with $r_2 = 1.023$ to zero leading to a first order phase transition driven by fluctuations. This is clearly a drawback of the theory. For $k_0 \neq 0$ (two-dimensional Ising model with dipolar interaction), the scenario is the same as that illustrated for $k_0 = 0$. For $k_0 = 0.05, 0.1, 0.15, 0.2$ $(J/g \simeq 126, 63, 42, 31)$, one finds $r_0^t = -1.7095, -1.7177, -1.7335, -1.7633$, and $r_2 = 0.973, 0.915, 0.848, 0.780$, respectively. The transition temperature obtained by this calculation is well described by the equation $T_t = (2.295 \pm 0.001) - (1.41 \pm 0.05)k_0^2$. The quadratic dependence of the first order transition temperature on g $(T_t = 2.295 - 55.7g^2)$ does not agree with the linear dependence obtained by the MC simulations (see Sec. III).

It is worthwhile to remember that the self-consistent (renormalized) Hartree-Fock approximation was extensively applied to magnetic (boson) Hamiltonians starting from the Heisenberg Hamiltonian in three dimensions.[17] The spin wave interaction taken into account by a variational approach leads to a first order phase transition. A self-consistent equation for the renormalization factor is found.

Two solutions exists for $T<T^*$, where the smaller one is always unstable with respect to the greater one. Comparing the free energy corresponding to the greater solution with the free energy of the disordered phase obtained from the constraint that the magnetization is zero, one finds that the transition temperature T_t is in good agreement with those estimated for the 3D isotropic Heisenberg cubic models for several spin S. Also in this case, however, the drawback is that at T_t, the magnetization jumps from a finite value to zero in a discontinuous way pointing out a first order phase transition at variance with the continuous phase transition of the 3D Heisenberg model. In conclusion, the first order phase transition driven by fluctuations seems to be an artifact of the Hartree self-consistent approach.

*Also at Istituto IMEM, CNR, Parco Area delle Scienze, 43100 Parma, Italy; rastelli@fis.unipr.it

[1] K. De'Bell, A. B. MacIsaac, and J. P. Whitehead, Rev. Mod. Phys. **72**, 225 (2000).
[2] S. A. Cannas, D. A. Stariolo, and F. A. Tamarit, Phys. Rev. B **69**, 092409 (2004).
[3] E. Rastelli, S. Regina, and A. Tassi, J. Appl. Phys. **99**, 08F708 (2006).
[4] E. Rastelli, S. Regina, and A. Tassi, Phys. Rev. B **73**, 144418 (2006).
[5] S. A. Cannas, M. F. Michelon, D. A. Stariolo, and F. A. Tamarit, Phys. Rev. B **73**, 184425 (2006).
[6] A. B. MacIsaac, J. P. Whitehead, M. C. Robinson, and K. De'Bell, Phys. Rev. B **51**, 16033 (1995).
[7] A. Abanov, V. Kalatsky, V. L. Pokrovsky, and W. M. Saslow, Phys. Rev. B **51**, 1023 (1995).
[8] I. Booth, A. B. MacIsaac, J. P. Whitehead, and K. De'Bell, Phys. Rev. Lett. **75**, 950 (1995).
[9] W. Selke, Phys. Rep. **170**, 213 (1988).
[10] R. Czech and J. Villain, J. Phys.: Condens. Matter **1**, 619 (1989).
[11] M. S. S. Challa, D. P. Landau, and K. Binder, Phys. Rev. B **34**, 1841 (1986); A. Billoire, R. Lacaze, A. Morel, S. Gupta, A. Irbäck, and B. Petersson, *ibid.* **42**, 6743 (1990).
[12] A. E. Ferdinand and M. E. Fisher, Phys. Rev. **185**, 832 (1969).
[13] S. A. Brazovskii, Zh. Eksp. Teor. Fiz. **68**, 175 (1975) [Sov. Phys. JETP **41**, 85 (1975)].
[14] M. Grousson, V. Krakoviack, G. Tarjus, and P. Viot, Phys. Rev. E **66**, 026126 (2002).
[15] M. Grousson, G. Tarjus, and P. Viot, Phys. Rev. E **64**, 036109 (2001).
[16] W. Selke, Z. Phys. B: Condens. Matter **43**, 335 (1981).
[17] M. Bloch, Phys. Rev. Lett. **9**, 286 (1962); J. Appl. Phys. **34**, 1151 (1963).